C Journal of Carbon Research

MDPI

Article

Membranes of Multiwall Carbon Nanotubes in Chitosan–Starch with Mechanical and Compositional Properties Useful in Li-Ion Batteries

Yoxkin Estévez-Martínez [1], Enrique Quiroga-González [2,*], Erick Cuevas-Yañez [3], Sergio Durón-Torres [4], Daniel Alaníz-Lumbreras [5], Elizabeth Chavira-Martínez [6], Rubén Posada-Gómez [7], Jeremias Bravo-Tapia [1] and Víctor Castaño-Meneses [8]

1 Instituto Tecnológico Superior de Acatlán de Osorio, Tecnológico Nacional de México, Acatlán de Osorio 74949, Puebla, Mexico; yoxkin.estevez.martinez@itsao.edu.mx (Y.E.-M.)
2 Institute of Physics, Benemérita Universidad Autónoma de Puebla (BUAP), Puebla 72570, Puebla, Mexico
3 Center for Research in Sustainable Chemistry, Autonomous University of Mexico State, Toluca 50200, Edo. de México, Mexico
4 Academic Unit on Chemical Sciences, Universidad Autónoma de Zacatecas, Zacatecas 96160, Zacatecas, Mexico
5 Faculty of Electrical Engineering, Universidad Autónoma de Zacatecas, Zacatecas 98000, Zacatecas, Mexico
6 Instituto de Investigaciones en Materiales, Universidad Nacional Autónoma de México, Mexico City 04510, Mexico City, Mexico
7 Instituto Tecnológico de Orizaba, Tecnológico Nacional de México, Orizaba 94320, Veracruz, Mexico
8 Center of Applied Physics and Advanced Technology, Universidad Nacional Autónoma de México, Juriquilla 76230, Queretaro, Mexico
* Correspondence: equiroga@ieee.org; Tel.: +52-2222295500 (ext. 2061)

Abstract: This work reports on membranes of a combination of chitosan–starch with lithium-modified multiwall carbon nanotubes. One of the most important contributions of this article is the functionalization of the surface of multiwall carbon nanotubes by means of an accessible technique that allows for high grafting yields of lithium and their incorporation into a polymeric matrix. The natural compounds chitosan and starch were used as a support to embed the nanotubes, forming membranes with good mechanical stability. A thorough characterization via Raman, infrared and X-ray photoelectron spectroscopies, transmission and scanning electron microscopies and dynamic mechanical analysis is presented here, as well as electrochemical characterization. The composition, structure and mechanical stability of the membranes make them viable candidates to be used as anodes sustainable Li-ion batteries.

Keywords: lithium grafting; mechanical stability; composite membrane; lithium-ion battery; multiwall carbon nanotubes; chitosan–starch

check for updates

Citation: Estévez-Martínez, Y.; Quiroga-González, E.; Cuevas-Yañez, E.; Durón-Torres, S.; Alaníz-Lumbreras, D.; Chavira-Martínez, E.; Posada-Gómez, R.; Bravo-Tapia, J.; Castaño-Meneses, V. Membranes of Multiwall Carbon Nanotubes in Chitosan–Starch with Mechanical and Compositional Properties Useful in Li-Ion Batteries. *C* **2023**, *9*, 87. https://doi.org/10.3390/c9030087

Academic Editors: Jandro L. Abot and Giuseppe Cirillo

Received: 18 June 2023
Revised: 21 August 2023
Accepted: 31 August 2023
Published: 8 September 2023

1. Introduction

Lithium-ion batteries (LIBs) dominate the market for portable electronic devices and are becoming increasingly important in other markets, such as electric vehicles [1–3]. However, many issues are being investigated to improve their security, efficiency and cost. One of the most promising approaches for improving the efficiency of this type of battery is the use of polymer electrolytes [4,5]. The carrier transport properties of common ionic liquids are very comparable to those of a polymer electrolyte [6], with the particularity that the polymer can be prepared as a membrane, providing mechanical support and stability to the cells. A solid electrolyte in a battery cell separates the electrodes, avoiding short circuits but allowing for the transport of specific ions (Li^+) from one electrode to the other at acceptable operating speeds. Similar characteristics are necessary for electrolytes for other applications, like proton-conductive materials used in fuel cells [7]. The electrolytes are required to exhibit high ionic conductivity and, at the same time, provide mechanical strength. This is

the case of multivalent phosphate cross-linked chitosan biopolymer membranes in borohydride fuel cells [8], biodegradable polystyrene sulfonated-lignosulfonate polymers as an electrolyte in fuel cell membranes [9] and, recently, conductive polymers within a hydrogel matrix to obtain synthetic hydrogels with characteristics for applications, such as artificial biological tissues, flexible electronics and conductive membranes [10]. Designing new engineered electrolytes like those is a challenge [11]. Other classic examples of such membranes are those based on coordination compounds using high-molecular-weight polymers and *Li* salts, like $LiClO_4$ or $LiN(CF_3SO_2)_2$. Examples of these polymers in the literature are polyethylene oxide, polypropylene oxide, polybis, methoxy ethoxyethoxy-phosphazene, polydimethyl siloxane, polyacrylonitrile, polymethyl methacrylate, polyvinyl chloride and polyvinylidene fluoride [6,12]. Most of the synthetic polymers mentioned above are difficult to degrade, causing environmental pollution problems. Because of this, today, there is an interest in natural polymers (carbohydrates), which degrade naturally in a normal environment in a short period of time. Such polymers are commonly referred to as biopolymers [13,14]. Research on the use of biopolymers as an electrolyte is currently highly competitive but represents a fertile area for future work [13,15]. This is the case with multivalent phosphate cross-linked chitosan biopolymer membranes in borohydride fuel cells [8], biodegradable polystyrene sulfonated-lignosulfonate polymers as an electrolyte in fuel cell membranes [9] and, recently, conductive polymers within a hydrogel matrix to obtain synthetic hydrogels with characteristics for applications, such as artificial biological tissues, flexible electronics and conductive membranes [10].

Carbon nanotubes as anodes in lithium batteries were used in a study from two decades ago. Two of the first works were one where the electrochemical discharge capacity of single-walled carbon nanotubes exceeded 1300 mAh/g after 30 charge/discharge cycles applying a current density of 20 $\mu A/cm^2$ [16] and a Japanese review where they concluded that single-walled carbon nanotubes have a high capacity of up to 3611 mAh/g [17]. On the other hand, in the literature, one can also find reviews that talk about the use of multiwall carbon nanotubes as electrodes, introducing other materials, like Mn_3O_4, $CoFe_2O_4$, Fe_xO_y, *Sn* and *CoSn*, between carbon walls exhibiting capacities ranging from 100 to 1000 mAh/g [2]. Additionally, in one of the latest publications, carbon nanotubes synthesized from used cooking oil at 900 °C showed excellent performance as anodes in a *Li*-Ion battery with a capacity of 213.75 mAh/g in cycle 30 [18]. In recently published work, we found that some researchers designed nanoporous nanocomposites of silicon microparticles with carbon nanotubes (PSI-CNTs) that offer a high specific capacity of 3210.1 mAh/g at a rate of 1/15 C. Their initial coulomb efficiency (CE) is 87.3%, but after 100 cycles, the capacity stabilizes above 2000 mAh/g, and the CE is 99.5% [19]. In recent studies, carbon nanotubes (CNTs) have been used as promising materials in different applications. Christwardana et al. [20] developed a photo-bioelectrochemical cell with a CNT-chlorophyll photo-biocatalyst, generating photo-currents 6-times higher than the current in darkness. On the other hand, Liu [21] presented a composite of polymer-CNT nanofibers as an anode for Li-ion batteries with a reversible capacity of 1105.2 $mAhg^{-1}$ and almost 100% columbic efficiency. Meanwhile, Li et al. [22] reported defect-rich sulfur-doped short amorphous carbon nanotubes (SACTs-S) with a high reversible capacity of 1608.7 $mAhg^{-1}$ at 50 mAg^{-1} and 538.0 $mAhg^{-1}$ over 2500 cycles at 2000 mAg^{-1}. This remarkable performance demonstrates the potential of CNT-based materials for future energy applications.

With the aim to embed CNTs in a polymeric electrolyte, good candidates were searched among biopolymers, finding that cellulose, starch, chitosan, agar, pectin and gelatin are good options [23]. For example, solid electrolytes based on polymeric pectin are used for the storage of anionic polysaccharide and ammonium iodide salt, exhibiting their maximum ionic conductivity (4.5×10^{-3} S/cm) at room temperature [24]. Similarly, a polymeric electrolyte based on corn starch with different percentages of sodium bisulfite ($NaHSO_3$) shows an ionic conductivity of 2.22×10^{-4} S/cm at room temperature [25]. On the other hand, biopolymers such as chitosan and starch have been studied by different authors in

this context [26–28], explaining their properties in detail. Furthermore, some authors have proposed using them as a matrix for carbon nanotubes [29–31]. The ionic conductivity of chitosan was found to be as high as 10^{-4} S/cm after 1 h hydration when it was prepared as membranes [32] and 2.1 × 10^{-3} S/cm when it was prepared as ionogel electrolyte with cellulose [33]. On the other hand, starch is not far behind, being an excellent electrolyte when mixed with other materials. This is the case of potato starch with $Mg(ClO_4)_2$, which exhibited high ionic conductivity (2.01 × 10^{-2} S/cm), low relaxation time (55 µs) and a wide voltage window of electrochemical stability (about 3 V) [34]. Another case is that of flexible electrolyte membranes of nanocomposites of polyethylene oxide/starch nanocrystals complexed with $MgBr_2$ salt, with an ionic conductivity of 1.16 × 10^{-6} S/cm at room temperature [35]. More recently, poly(ε-caprolactone) membranes have been synthesized with chitosan and bis(trifluoromethanesulfonyl)imide salt (LiTFSI to 50 wt%) to obtain an ionic conductivity of 7.7 × 10^{-4} S/cm [36].

However, the use of combinations of chitosan and starch as solid electrolytes is new, taking advantage of the properties of these polymers. Chitosan provides strength, while starch provides good ionic transport. There is a report on an unplasticized solution of starch–chitosan doped with NH_4I, which had a good conductivity at room temperature of up to (3.04 ± 0.32) × 10^{-4} S/cm [37]. In a different work, the synthesis of a biodegradable solid polymer electrolyte of a mixture of chitosan and potato starch, plasticized with glycerol and lithium perchlorate ($LiClO_4$), showed a maximum ionic conductivity of 6.5 × 10^{-4} S/cm [38]. In a more recent report, a chitosan–starch solid biopolymer with 9 wt% of oxidized graphene showed a maximum conductivity of around 10^{-3} S/cm [39].

Combining these natural polymers with carbon nanotubes as electrodes provides a novel and eco-friendly approach to designing LIBs with improved performance, stability and reduced environmental impact. Moreover, the combination of chitosan and starch as solid electrolytes takes advantage of their respective strengths, resulting in a promising electrolyte matrix with enhanced ionic transport capabilities [39,40]. This composite represents an innovative and sustainable solution to address some challenges of lithium-ion batteries. For this reason, this article reports on the production of carbon nanotube membranes (*MWNTs*) embedded in a chitosan/starch matrix, with the intention of using them in a future development as an electrode for lithium-ion batteries. Furthermore, two unconventional routes for lithium-modified multi-walled carbon nanotubes with lithium hydroxide (LiOH) are presented: reflux (RLi) and sonication (SLi). The compositional, mechanical and electrochemical properties of the composites are thoroughly studied.

2. Materials and Methods

2.1. Materials Synthesis

Multiwall carbon nanotubes (*MWNTs*) prepared via chemical vapor deposition were obtained from Sun Nanotech Co. (Nanchang City, Jiangxi province, China) The *MWNTs* had a diameter from 10 to 30 nm and a length of 1 to 10 µm, with a purity > 90% and a surface area of 90 to 350 m^2/g [41]. The other reactants were purchased from Sigma-Aldrich Co. LLC. (San Luis, MI, USA). These reagents did not undergo any further purification.

According to the literature cited [42–47], the purification/oxidation of the *MWNTs* was achieved in a 3:1 mixture of HNO_3 (75%) and H_2SO_4 (98%) at 85 °C for 3 h in a reflux process. The resulting material was vacuum washed to a neutral pH with deionized water. The product is called *MWOHs* in this work. Afterwards, it was lithium-modified in two different ways, according to the study of [48].

Reflux-lithiated nanotubes (RLi) were synthesized using a carefully controlled procedure involving a specific weight ratio of 6:1 w/w between *MWOHs* and LiOH. LiOH was dissolved in an aqueous solution with a concentration of 0.01 M. The synthesis process was conducted in a round-bottom flask equipped with a reflux condenser. The flask was charged with the precursor mixture, and a stirring bar magnet was employed to ensure homogeneity. The reaction mixture was then subjected to reflux conditions, maintaining a temperature of 75 °C for a duration of 2 h. During this period, chemical reactions took

place, leading to the formation of lithiated nanotubes. Subsequent to the reaction, the resulting material underwent thorough purification. Vacuum washing with deionized water was employed, with multiple wash cycles being conducted until the pH of the solution reached a neutral state. This step was crucial to remove any residual reactants or byproducts. Finally, the obtained lithiated nanotubes were carefully collected and preserved in a hermetically sealed glass jar to prevent any unintended interactions with the surrounding environment. In contrast, the synthesis of sonicated-lithiated nanotubes (SLi) involved a different approach. The same precursor materials, with the same weight proportions, were used. However, instead of refluxing, the synthesis took place under sonication conditions. The precursor mixture was placed in a flask equipped with an ultrasonic homogenizer. The mixture was subjected to ultrasonic waves at room temperature for a duration of 2 h. The sonication process facilitated the incorporation of lithium ions into the nanotube structure. Similar to the reflux method, the resulting sonicated-lithiated nanotubes were subjected to thorough purification through vacuum washing with deionized water. The purification process was repeated until the pH of the solution reached neutrality, ensuring the removal of any residues. The purified nanotubes were then securely stored in an airtight glass jar to prevent any degradation or contamination. These distinct synthesis approaches, reflux and sonication, provided two sets of lithiated nanotubes (RLi and SLi) with controlled properties. These synthesized materials held promise for various applications due to their unique structural and electrochemical characteristics.

The polymer electrolyte was prepared with a mixture of chitosan–starch solutions. According to previous research [15,49–51], the chitosan (Ch) solution (2% m/v) was prepared by dispersing chitosan in an acetic acid aqueous solution (1% v/v) and then stirring at 100 rpm. After the chitosan was completely dispersed, the solution was sonicated for 15 min to break any air bubbles present and then allowed stand for 1 h. The starch (St) solution (2% m/v) was prepared dispersing starch in glycerin and heating above its gelatinization temperature (90 $\pm$ 2 °C) [52], continuously stirring at 100 rpm for 20 min. The solution was then cooled down to room temperature by ceasing heat and stirring. Finally, the chitosan–starch films (*ChSt*) were obtained mixing equal volumes of chitosan and starch solutions and then sonicating to homogenize.

The complete membranes for each batch of *MWNTs* (pristine *MWNTs*, *MWOHs*, RLi and SLi) were prepared by dispersing them within the chitosan–starch polymer matrix at a concentration of 0.025% w/v. The dispersion, totaling 4.55 $\times$ 10^{-3} L m^{-2}, was poured into a polyethylene container. Ultrasonic agitation was employed for 120 s, accompanied by mechanical vibration. The resulting dispersion was subsequently air-dried at room temperature in polystyrene molds within a fume hood for a duration of 24 h. Following this process, the samples underwent characterization. An overview of the complete fabrication procedure is provided in Figure 1.

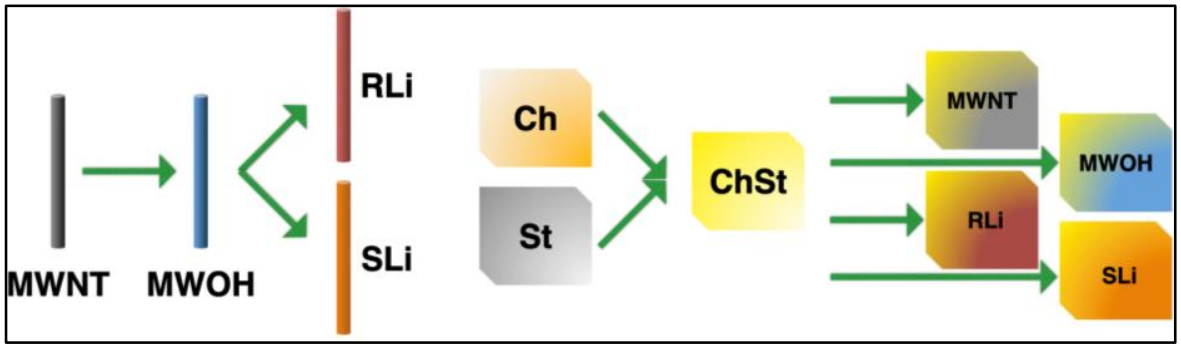

Figure 1. Schematic of the fabrication process of the different modifications to the carbon nanotubes and the synthesis of the chitosan–starch matrix and the different nanocomposites.

2.2. Characterization

For the characterization of *MWNTs*, *MWOHs*, R*Li* and S*Li*, the analyses of X-ray photoelectron spectroscopy (XPS) were performed with a JEOL JPS-9200 Photoelectron Spectrometer (ESCA) (Tokyo, Japan). Infrared (FTIR) spectra were recorded using a Vector 33 Bruker spectrophotometer (Billerica, MA, USA) at 32 scans, with a resolution of 4 cm^{-1}. Solid samples were embedded in *KBr* disks. Raman spectra were recorded with a Dilor LabRAM Micro-Raman with a resolution of 0.5 cm^{-1}, with a 514.5 nm laser with 15 s of integration time. High-resolution transmission electron microscopy (HRTEM) of *MWNTs* and *MWOHs* was performed with a JEOL–JEM 2010FEG instrument (Tokyo, Japan); on the other hand, micrographs of R*Li* and S*Li* were recorded with a JEOL–JEM 2200FS instrument (Tokyo, Japan). All the samples for microscopy were prepared by depositing droplets of a suspension of the studied materials on 100-mesh microscope gold grids.

All the chitosan–starch examples were characterized via dynamic mechanical analysis (DMA) with the objective of analyzing the thermo-mechanical properties of the polymer electrolyte. Dynamic mechanical analysis (DMA) was recorded using an RSA III of TA instruments (New Castle, DE, USA). Measurements were run using tweezers to tension in a temperature range from 30 °C to 350 °C, with a frequency of 1.0 Hz. Scanning electronic microscopy (SEM) was recorded in a SEM JEOL 5200 (Tokyo, Japan) with 5.0 of resolution to 25 kV. Infrared (FTIR) spectra were recorded in a Vector 33 Bruker spectrophotometer (Billerica, MA, USA) at 32 scans, with a resolution of 4 cm^{-1}.

The electrochemical measurements were performed using an EG&G PAR VersaSTAT 3 Potentiostat/Galvanostat (Princeton, NJ, USA). Cyclic voltammetry studies were performed from −2.5 to 2.5 V, at a scan rate of 50 mV/s. Electrochemical impedance spectroscopy (EIS) experiments were carried out in potentiostatic mode in the 1 MHz to 1 Hz frequency range. The impedance spectra were registered with a logarithmic data collection scheme at 10 steps per decade at open-circuit potential with a small signal amplitude of 10 mV.

3. Results and Discussion

The results obtained are presented below, separating them into two sections. First, the results of the characterization of the different reinforcement used are shown, such as carbon raw and oxidized nanotubes (*MWNTs* and *MWOHs*), as well as lithium-modified ones (R*Li* and S*Li*). Subsequently, the characterization of the chitosan–starch (*ChSt*) membranes with the different kinds of nanotubes is shown.

3.1. Characterization of Carbon Nanotubes via FTIR

Figure 2 shows the normalized spectra of the *MWNTs* after the different treatments. It is possible to see the characteristic FTIR peaks of the carbon nanotubes [53–57], which describe the normal modes of vibration at ~1632 cm^{-1} for E_{1u} and ~800 cm^{-1} for A_{2u} in multiwall carbon nanotubes (*MWNTs*) in all cases. Additional bands can be identified in oxidized carbon nanotubes (*MWOHs*, R*Li*, S*Li*) between 1750 and 1550 cm^{-1} for *v*(*C*=*O*), 1466 cm^{-1} for *δ*(*O*–*H*) and between 1300 and 950 cm^{-1} for *v*(*C*–*O*) due to vibrations of the carboxyl groups and at 3443 cm^{-1} for isolated surfaces of v_s(*OH*) [54,57–59]. The presence of lithium in the samples could be evidenced through the interaction of *Li* with oxygen and carbon. According to some authors [60–65], the molecular vibration bands suggest the presence of R*OCO*$_2$*Li*, Li_2O, Li_2CO_3, R*OLi* and *LiOH*. *O*–*H* bands are visible at 3700–3100 cm^{-1}, being broader in the lithium-modified samples than in the pristine *MWOHs*. st(*C*–*H*) at 3000–2800 cm^{-1} and st(*C*–*O*) at 1064 cm^{-1} correspond to R*OCO*$_2$*Li* and R*OLi*, respectively. st(*Li*–*O*) of the Li_2O is visible at 530 and 476 cm^{-1}. Additionally, the *C*–*O* band at 880 cm^{-1} may originate from Li_2CO_3. Finally, the bending vibrations CH_2 at 1466 cm^{-1} and *C*=*O* symmetric at 1628 cm^{-1} and asymmetric at 1367 cm^{-1} vibrations indicate the presence of R*OCO*$_2$*Li*. These results indicate that lithium ions are interacting with carbon nanotubes at these normal modes of vibration, thus promoting their use as electrodes in lithium batteries [66].

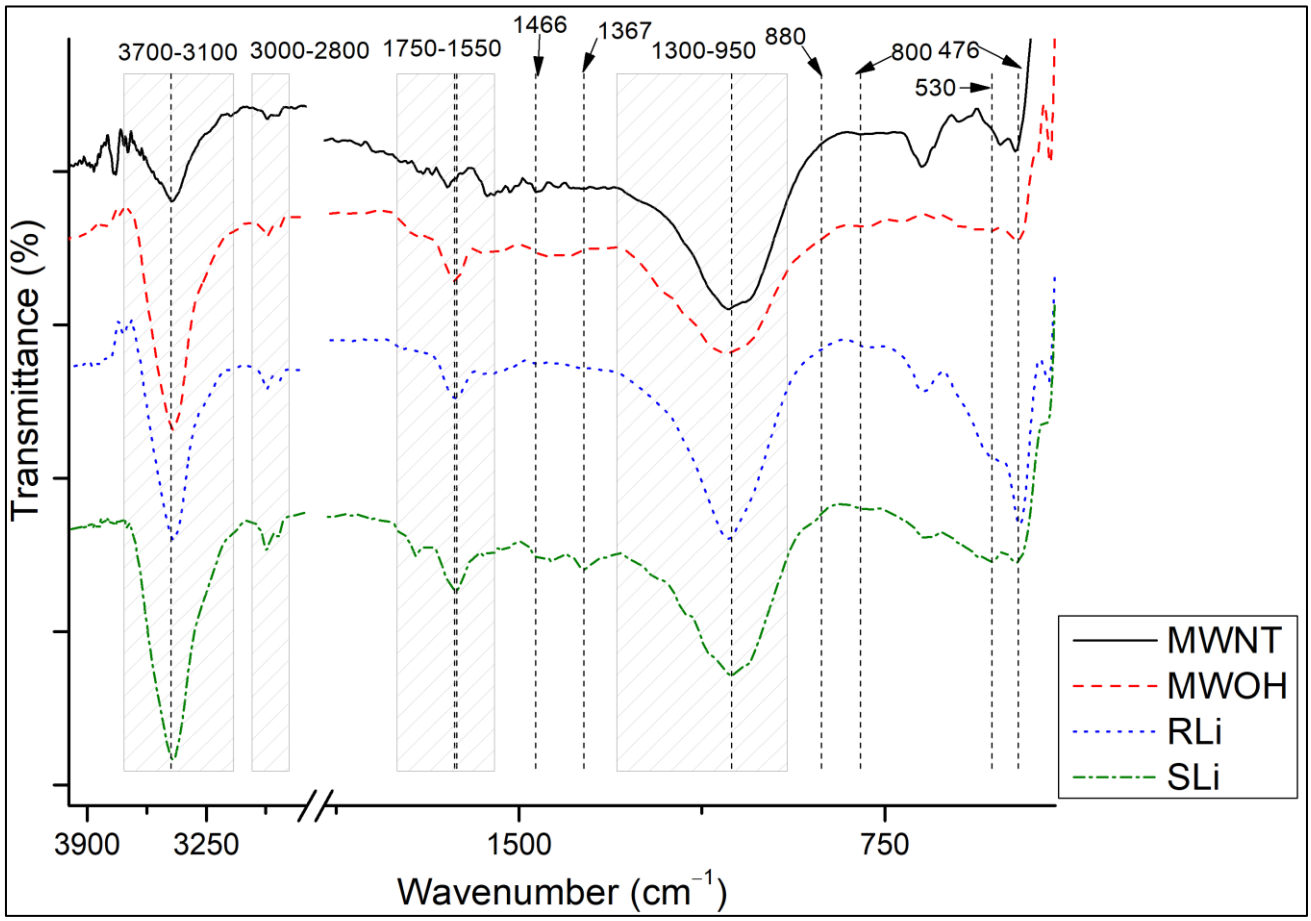

Figure 2. FTIR of different modifications of multiwall carbon nanotubes: raw (*MWNTs*), oxidized (*MWOHs*) and lithium-modified (R*Li* and S*Li*).

3.2. Characterization of Carbon Nanotubes via Raman Spectroscopy

Raman spectra of *MWNTs*, *MWOHs* and lithium-modified multiwall carbon nanotubes (R*Li* and S*Li*) are shown in Figure 3. For some authors, Raman spectroscopy is considered the fingerprint of carbon nanotubes [67–73], allowing one to produce a deep analysis of the oxidation, purification and modification of the structure of their outer walls. The most prominent peaks of the spectra at ~1570 cm^{-1} (G band), ~1340 cm^{-1} (D band) and ~2684 cm^{-1} (G′ band) and their overtones found as small peaks at 1233 and 2898 cm^{-1} are all attributed to carbon [59,71,73–82] and give a good indication of the state of CNTs. In some publications [83,84], the G band (the name G comes from "Graphite") is used as an indicator of purity since the CNTs should ideally present a graphitic order with carbon in sp^2 hybridization. When broken bonds are present, carbon can hybridize sp^3, giving rise to the D band (the name D comes from "Defect"). Thus, this band can be used to identify if there are dangling bonds or impurities on the surface of the CNTs [85,86]. The ratio between the intensities of these two bands gives a hint of the purity of carbon nanotubes, but it says nothing of the kind of material (graphite, fullerene, CNTs); for this last thing, the FWHM of the peaks should also be considered (e.g., the FWHM of graphite is usually larger than that of CNTs) [86]. In this work, to consider the width of the peaks, the area of the peaks was used instead of the intensity. The areas of the different peaks are tabulated in Table 1, for the different samples. The G′ band is related to the G band, whose intensity is proportional to the purity of the multiwall carbon nanotubes due to the absence of nanocarbons (disordered phase) in the samples [87]. The ratio between areas of the different peaks (G′/G, G′/D and D/G) was calculated, as shown in Table 1. The values suggest that the oxidation of *MWNTs* cured defects, since the ratio D/G decreases

and ratio G′/D increases. The small difference in G′/G values could be due to the removal of carbonaceous material during oxidation [88].

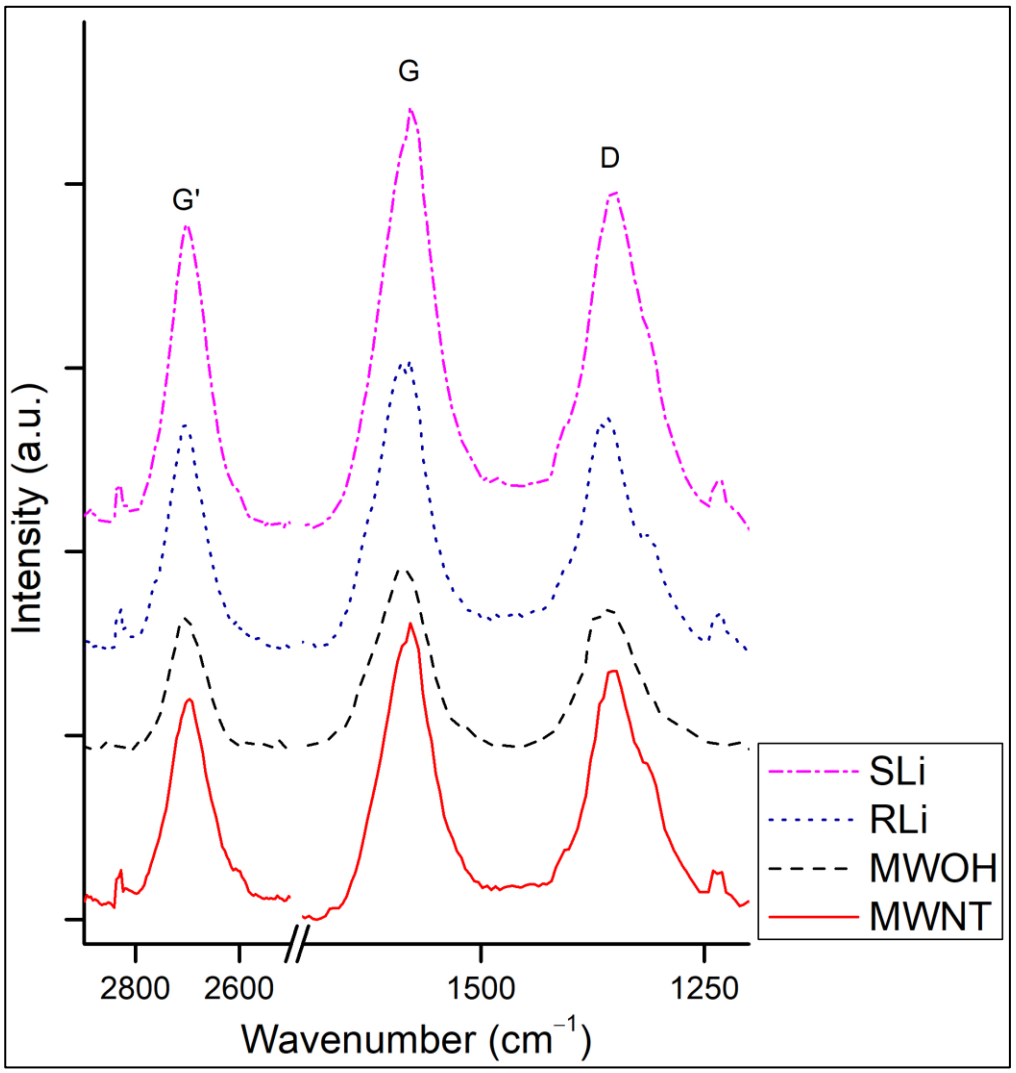

Figure 3. Raman spectra of different modifications of multiwall carbon nanotubes: raw (*MWNTs*), oxidized (*MWOHs*) and lithium-modified (R*Li* and S*Li*). The most significant bands (G′, G and D) are marked.

Table 1. Areas of the Raman bands and ratios between them for the different modifications of *MWNTs*.

Samples	D	G	G′	G′/G	G′/D	D/G
MWNTs	72,068	79,955	81,314	1.02	1.13	0.90
MWOHs	40,546	52,738	51,791	0.98	1.28	0.77
R*Li*	64,666	80,951	77,683	0.96	1.20	0.80
S*Li*	98,968	117,520	108,288	0.92	1.09	0.84

The samples intercalated with lithium show a drop in G′/D compared to *MWOHs* due to the decrement in the area of G′ caused by the exfoliating action of *LiOH*, which degrades carbonaceous materials [89,90]. The exfoliated surface of *MWNTs* is more reactive [91], which is positive for capturing *Li*-ions. Moreover, *Li*-ions can be intercalated in MWCNT's inner walls because of coulombic repulsion effects [92]. A significant decrement in the D/G ratio in comparison with the MWNTs is observed in the lithium-modified samples, in accordance with various publications [92–99], indicating a possible exfoliation of carbon nanotubes. It is also important to mention that the small peaks that appear in the spectra

refer to normal vibration modes that are affected in position due to the oxidation of multiwall carbon nanotubes [100]. Furthermore, the G′/G and G′/D are larger in RLi than in SLi, indicating that there is an increment in the G′ band with respect to the other bands in this sample [101]. The greater contribution of this band to the RLi spectrum could suggest a higher graphitic character of this sample, as this band is observed as an overtone of graphitic samples, and it is not affected by defects [102]. The graphitic nature of the sample, in addition to allowing for Li ion intercalation, enhances electron transfer, promoting its use as an electrode in lithium batteries [103]. SLi may have undergone a higher degree of oxidation during Li incorporation, as indicated with the higher proportion of the D band in this sample in comparison with RLi. This effect is common when oxidizing graphene [102].

3.3. Characterization of Carbon Nanotubes via XPS

XPS was employed to quantify the relative lithium content of RLi and SLi compared to carbon and oxygen, referencing MWNT and MWOH spectra for analysis. Carbon (C1s) exhibited binding energies within a range of 295 to 281 eV, oxygen (O1s) within 540 to 528 eV and lithium (Li1s) within 61 to 57 eV. The deconvolution of C1s, O1s and Li1s peaks was based on established data from previous XPS studies on lithium-modified multiwall carbon nanotubes [63,104–107]

In terms of the C1s peak, the hydroxyl (–OH at 286.6 eV) and carboxyl (–COOH at 288.6 eV) bands of lithium-modified multiwall carbon nanotubes were found to be more prominent compared to pure nanotubes. This phenomenon may be attributed to the presence of lithium carbonate. An increase in π-π^* electronic transitions (at 290.9 eV) in MWOHs indicated potential CNT wall exfoliation due to acids [57]. Conversely, lithium-modified nanotubes demonstrated reduced transitions, implying non-covalent interactions.

Regarding the O1s band, the intensity of carboxyl, carbonyl and carbonate bands were considered (–COOH at 531.2 eV, O=C at 532.1 eV, and C–O*–C=O at 534.3 eV). Comparing the spectra of RLi and SLi, one could observe that the contribution of C–O and C=O bands in SLi is much higher, indicating that the sample was oxidized due to the L incorporation method, as suggested by the Raman spectra. Nevertheless, both samples are well lithiated, as indicated by the presence of the Li_2CO_3 band at 56 eV. On the other hand, analyzing the Li 1s line, it is possible to observe the presence of Li^0 and Li_2O on lithited surfaces. Furthermore, strong electrostatic interactions between lithium ions and CNTs led to a decrease in the intensity of π-π^* transitions (at 290.9 eV) [104] in lithiated samples with respect to the non-lithiated samples. The presence of lithium indicated the potential of these samples for facilitating electrode-to-electrode transfer in lithium batteries. Figure 4 (subscripts A and B) provides an illustrative deconvolution of spectra encompassing the aforementioned bands according to different reports [108,109].

3.4. Characterization of Carbon Nanotubes via HRTEM

The HRTEM micrograph in Figure 5, of the as-received *MWNTs*, shows the walls of a multiwall carbon nanotube and other allotropic forms of carbon as impurities. An FFT pattern (Fast Fourier Transform) was obtained from two zones: “1” is part of a multiwall carbon nanotube and “2” belongs to graphite. In both areas, the FFT shows the presence of fine dots (defined peaks in the line scan), confirming the presence of ordered carbon. On the other hand, the diffuse rings in the FFT patterns and the corresponding wide peaks in the line scans indicate sections of low crystallinity due to impurities, likely corresponding to low-order graphite originating from *MWNTs* [110,111].

The HRTEM micrograph of *MWOHs* in Figure 6 clearly shows defects on the walls of the nanotubes. By analyzing two areas of these *MWOHs* micrographs with FFT, both display more diffuse spots, and the line scan shows a rather poor crystallinity, revealed by the wide peaks and low intensity of the central spot. This is a characteristic of defective CNTs exhibiting distorted layers [59,112], confirming the oxidation of the multiwall carbon nanotubes.

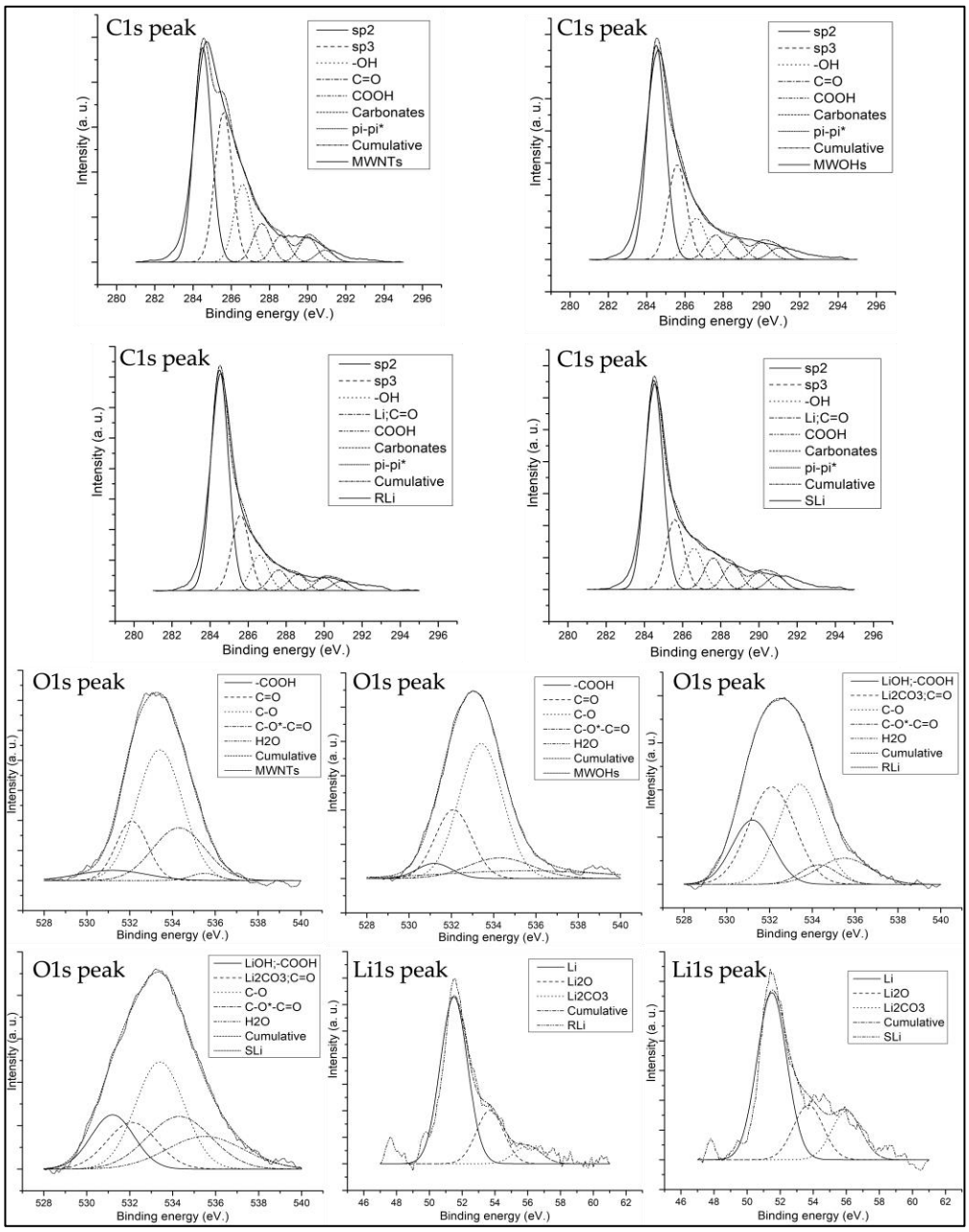

Figure 4. XPS spectra of C1*s*, O1*s* bands of *MWNTs*, *MWOHs*, R*Li* and S*Li* samples and *Li*1*s* band for *RLi* and *SLi* samples.

HRTEM micrographs and ED patterns of R*Li* and S*Li* are shown in Figure 7. From the micrographs, it is possible to see the presence of a higher amount of material covering the nanotubes in R*Li* than in S*Li*. This material must be Li^0 and Li_2O, as confirmed via XPS. In S*Li*, *Li* becomes more internal, forming Li_2CO_3. Thus, ultrasound induces the insertion of *Li*. The crystal planes of the nanotubes are evident in both cases, indicating that the crystallinity of the material remains, even after the oxidation and lithiation processes. In a recent publication [113], it was confirmed that the crystallinity of *MWNTs* increases after oxidation. The diffraction patterns indicate that the material is polycrystalline, in accordance with the HRTEM micrographs, showing bending crystalline planes. The two inner rings in the ED patterns originate in *MWNTs* [101,114]. The smallest one denotes the d-spacing of graphite oxide, which, in the present case, is 10.44 Å. The second ring corresponds to the d-spacing between (002) graphite planes, being, in the present case,

3.92 Å. The d values of outer diffuse rings (2.33, 1.91 and 1.38 Å) are in accordance with d values found for VAST-*MWNTs* [115], which, in XRD with Cu Ka, produce reflexes at 67.97°, 47.65° and 38.5° 2θ, respectively. These last values are characteristic of platinum, being from its (111), (200) and (220) planes [116]. Thus, the as-purchased VAST-MWNT contains *Pt*. Therefore, with this, we confirm that by analyzing the diffraction patterns of the HRTEM micrographs in the lithiated carbon nanotubes, we corroborate that they can be used as electrodes in lithium batteries, as has been previously reported [117].

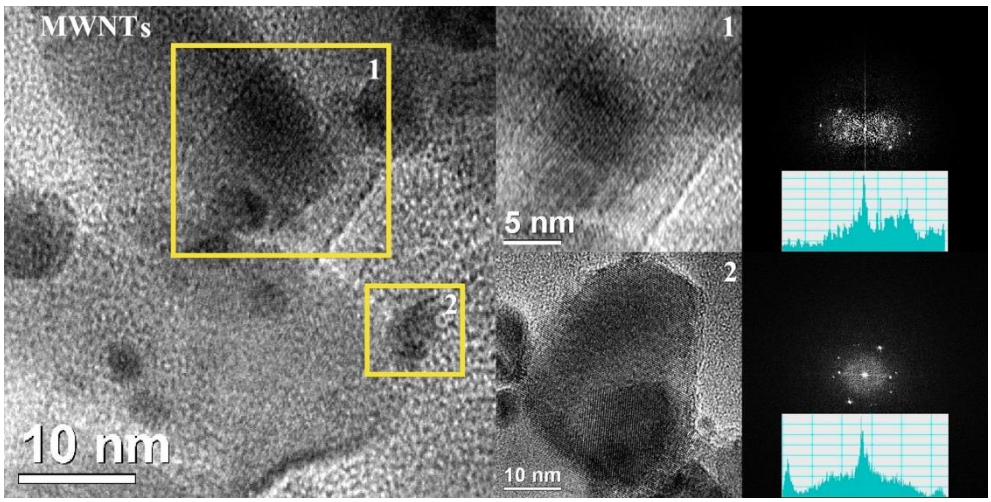

Figure 5. HRTEM (**left**) and FFT patterns (**right**) of multiwall carbon nanotubes (*MWNTs*) in different sections (1 and 2).

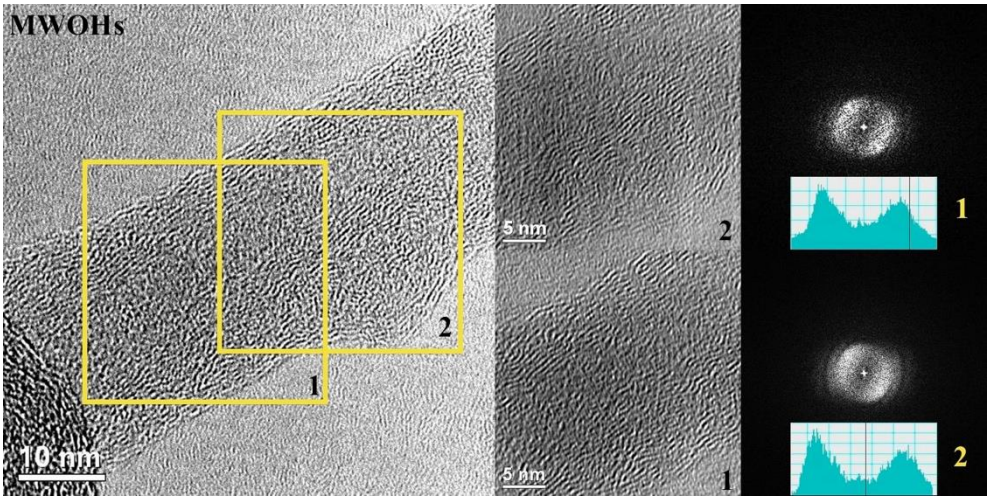

Figure 6. HRTEM (**left**) and FFT patterns (**right**) of oxidized multiwall carbon nanotubes (*MWOHs*) in different sections (1 and 2).

3.5. Characterization of the Chitosan–Starch (ChSt) Membranes via DMA

To test the mechanical properties of the polymeric matrix and how this property is improved by introducing multiwall carbon nanotubes, the membranes were characterized via dynamic mechanical analysis (DMA). Only the membranes with the lithiated nanotubes were omitted, due to the predominant amount of oxide groups linked to lithium, as confirmed via XPS characterization.

Dynamic mechanical analysis (DMA) was used to characterize the electrolyte *ChSt* and the nanocomposites of this electrolyte with *MWNTs* and *MWOHs*, with the purpose of giving an idea about the mechanical stability of the composites, away from the lithiation of the carbon nanotubes. DMA is a thermo-mechanical test where viscoelastic data of

the materials under test are collected at different temperatures [118,119]. Figure 8 shows the values of the modulus E′ at different temperatures. It is possible to observe that for *MWOHs*, E′ is around 445% the value of the other samples at 35 °C. Even at 200 °C, the E′ of this sample practically doubles that of chitosan–starch and is 1.6-times that of MWNTs.

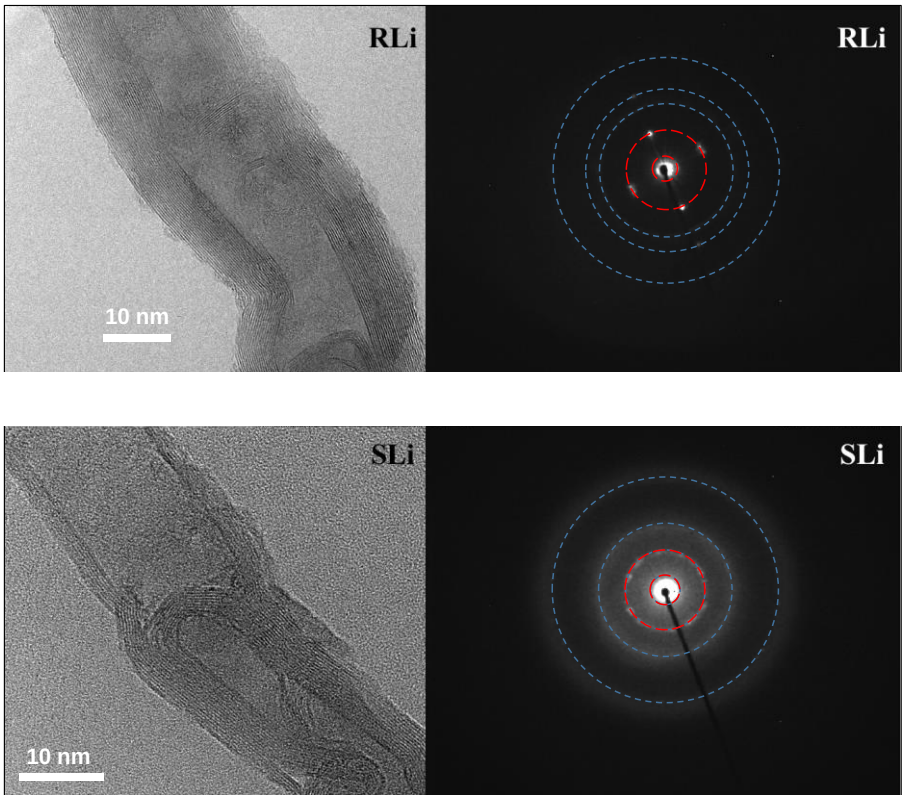

Figure 7. HRTEM (**left**) and ED patterns (**right**) of R*Li* and S*Li*.

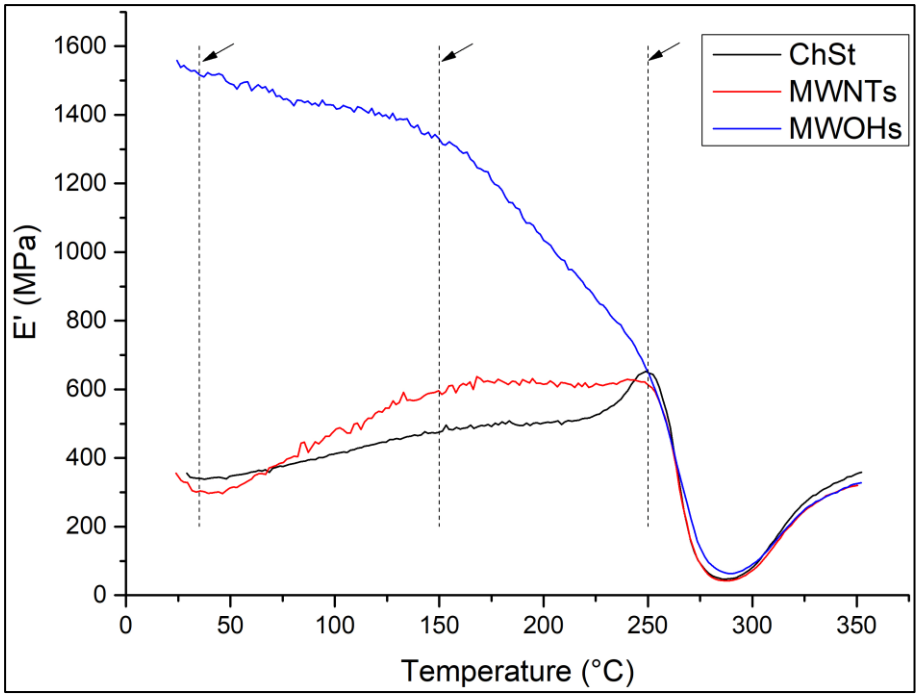

Figure 8. Storage modulus (E′) at different temperatures via dynamic mechanical analysis (DMA). The dashed lines and arrows indicate reference temperatures used for the discussion.

The fact that the storage modulus of the membrane increases as the temperature rises, up to the critical point of 250 °C, for ChSt and the membrane with MWNTs, is because there is an increment in crystallinity of the films produced by the arrangement of the starch molecules and because the interactions between the OH– groups of the glucose units and the H+ groups of the water molecules minimize [120]. The storage modulus increases linearly from 35 to 150 °C, but the slope of the curve is higher for MWNTs than for ChSt. Then, from 150 to 250 °C, there is a steady state for both samples, indicating that a maximum ordering is reached. On the other hand, when oxidized carbon nanotubes (MWOHs) are incorporated into the chitosan–starch film, a phenomenon similar to adding a plasticizer to the membrane is observed. As the temperature increases, the thermal energy begins to overcome these intermolecular forces. The polymer chains start to experience more vibrational motion and increased molecular mobility. This phenomenon is often referred to as "softening" or "rubbery behavior". As a consequence, the material becomes less rigid and more compliant, leading to a decrease in the storage modulus [121].

Through the relationship between the storage and loss modulus, the internal friction of materials can be determined, known as Tan (δ). High internal friction is reflected as high Tan (δ) values. Depending on the degree of adhesion between the phases, the internal energy is dissipated at the interface. Enhanced adhesion results in increased friction, as evidenced by a Tan (δ) value of 0.8 at 35 °C for the sample with MWOHs, while the other two samples exhibit a value of 0.55. Thus, oxidizing the *MWNTs* greatly enhances the adhesion properties between phases, probably due to *–OH* groups that promote hydrogen bonds. Stability in their mechanical properties gives us the confidence to use these materials in lithium batteries, as used in other reported works [122]. Sample MWOH was considered a model for RLi and SLi, taking into account that the oxygen content and the surface characteristics of these samples are similar, as evidenced through FTIR and Raman spectroscopies and XPS.

3.6. Characterization of the Chitosan–Starch (ChSt) Membranes via FTIR

For the nanocomposites of carbon nanotubes in a chitosan–starch matrix, when we compare the different FTIR spectra, they are very similar between the *ChSt* with the different modifications of multiwall carbon nanotubes: raw (*MWNTs*), oxidized (*MWOHs*) and lithium-modified (*CRLi* and *CSLi*). For this reason, we only show the FTIR spectra of starch, chitosan and their mixture in Figure 9, as shown in other reports, where the reinforcement of nanostructures in polymeric matrices is practically imperceptible [123]. We can remember that they have a reinforcement in the polymer matrix of chitosan–starch at 0.025% w/v. For starch, a band at 3274 cm^{-1} of st(*O–H*) of glycosidic chains is present. Also characteristic of starch, peaks at 2921 and 2926 cm^{-1} are present. These are st(*CH*) vibrations associated with the methine ring hydrogen atoms [124–127]. For chitosan, the peak at 3496 cm^{-1} is due to the *OH* group (ν_{OH}), the one at 3345 cm^{-1} is due to *NH* group-stretching vibration (ν_{NH}) and the ones at 2926, 2873, 1421, 1322 and 1249 cm^{-1} are due to symmetric or asymmetric CH_2 stretching vibrations attributed to pyranose rings (ν_{CH}). The peak at 1646 cm^{-1} is due to *C=O* in amide groups (amide I band). The one at 1593 cm^{-1} is due to NH_2 bending vibration in an amino group (δ_{NH2}). The peak at 1421 and 1322 cm^{-1} is due to vibrations of *OH* in a *CH* ring, the one at 1381 cm^{-1} is due to CH_3 in amide group, the one at 1249 cm^{-1} is due to *C–O* group, the one at 1156 cm^{-1} is due to *–C–O–C–* in glycosidic linkage, the ones at 1096 and 1030 cm^{-1} are due to *C–O* groups (ν_{C-O}) in amides and the one at 897 cm^{-1} is due to the CH_3COH group [128–130]. A linear combination of the spectra of starch, chitosan and *MWNTs* is observed in the composites, depending on their composition. Although these reinforcements could be imperceptible in this FTIR characterization, their use as electrolytes [123] or electrodes [131] for their proposal in lithium batteries has been reported.

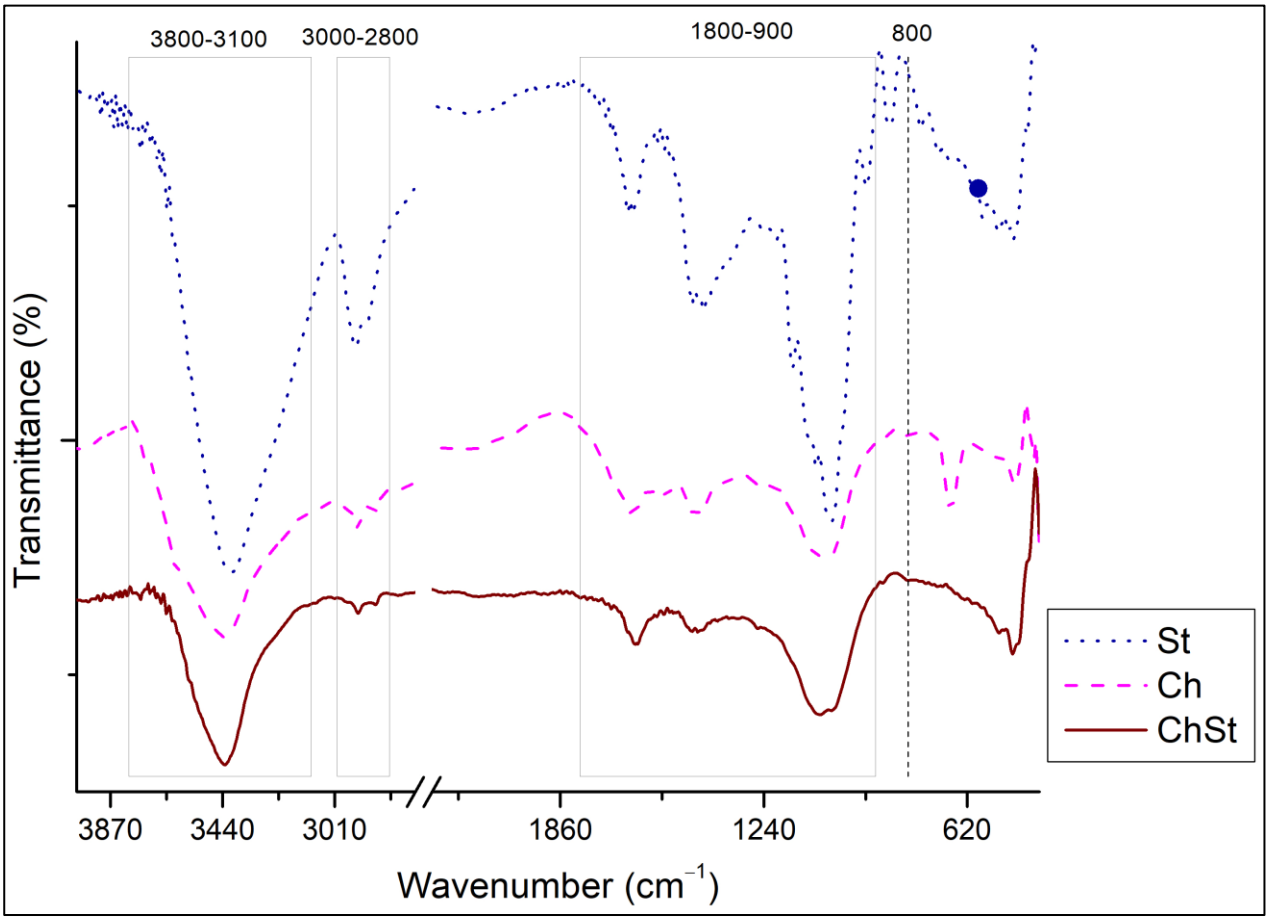

Figure 9. FTIR of starch (St), chitosan (Ch) and chitosan–starch (*ChSt*).

3.7. Characterization of the Chitosan–Starch (ChSt) Membranes via SEM

The SEM micrographs in Figure 10 display the surface (S) and cross-sectional (C) morphologies of the *ChSt*, *MWNTs* and *MWOHs* nanocomposite samples. The *ChSt* sample exhibits a smooth and continuous surface in both morphologies, indicating a homogeneous structure without observable fissures. In contrast, the samples reinforced with raw carbon nanotubes (*MWNTs*) and oxidized carbon nanotubes (*MWOHs*) display distinct slit formations in the cross-sectional views, indicative of the incorporation of nanotubes into the membrane matrix.

Regarding the absence of SEM images for the lithiated carbon nanotubes (RLi and SLi), there is a specific rationale for this omission. Lithiated nanotubes were not included in the SEM characterization due to their relatively low percentage of reinforcement in the composite. Given the minute amount of lithium-modified nanotubes, any observable morphological differences would likely be negligible and difficult to distinguish from the background matrix. Therefore, the decision was made to focus the SEM analysis on the most significant reinforcements, *MWNTs* and *MWOHs*, to provide clearer insights into the composite structure.

Additionally, it is important to note that the organic nature of the samples required a thin gold coating prior to SEM imaging. This coating was applied to enhance the conductivity of the samples and minimize the risk of charging effects, ensuring accurate and reliable imaging under the electron beam.

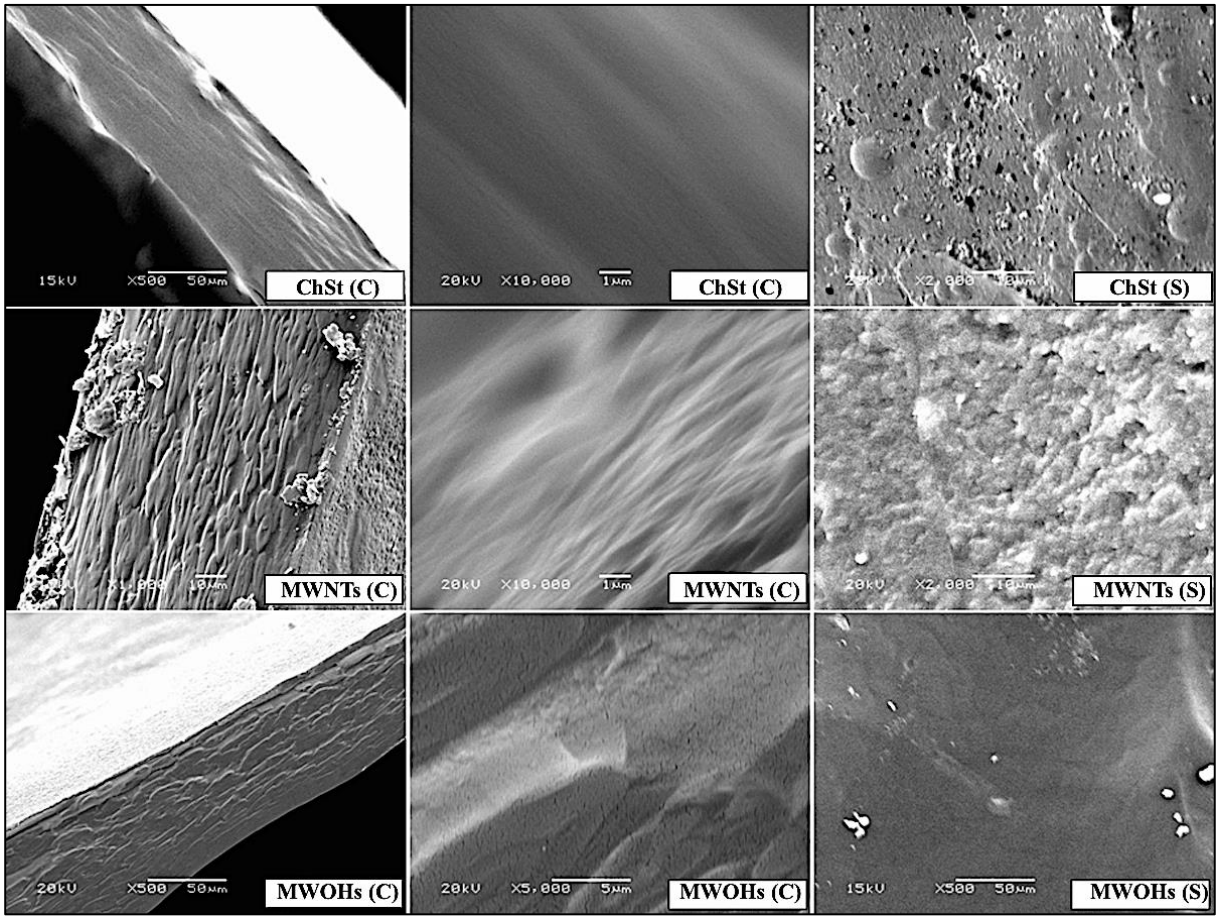

Figure 10. Scanning electron microscopy (SEM) of the surface (S) and cross-section (C) of biopolymer chitosan–starch (*ChSt*) with *MWNTs* and *MWOHs* reinforced.

3.8. Electrochemical Characterization of the Chitosan–Starch (ChSt) Membranes

Figure 11 depicts the assembly of the device for electrochemical characterization, which consists of two aluminum electrodes sandwiching the chitosan–starch (*ChSt*) membrane of 1 × 1 cm. The cell was hot sealed with polyethylene terephthalate. The tests were performed with a membrane of reflux-lithiated nanotubes (RLi), considering that these nanotubes are less oxidized than the SLi and may enhance electron transfer when used electrochemically. A membrane of oxidized carbon nanotubes (*MWOHs*) was also measured as a reference.

Figure 11. Device for electrochemical characterization.

Figure 12 shows cyclic voltammetry curves of using the assembly from Figure 11 and membranes of MWOHs and RLi. The third cycle is shown for both samples. As can be seen, the voltammograms are relatively symmetrical, as expected when using a symmetric electrochemical cell. Both the membranes with MOWHs and RLi present pairs of oxidation and reduction peaks close to 0 V. The difference in potential either between oxidation or

oxidation peaks is of 0.84 V for MWOHs and 0.75 V for RLi. The peaks of the RLi sample are just shifted, having a lower potential difference between oxidation and reduction peaks (the processes are facilitated). This could be related to a lower ohmic drop. In fact, the parallel resistance, most probably related to the charge transport in the electrolyte, is lower in the sample with lithium. This can be denoted in the impedance spectra of cells with different membranes (See Figure 13). As can be observed, the diameter of the semicircle is smaller for the RLi sample. This is associated with parallel resistance. Then, the conductivity of the membrane is enhanced due to the presence of Li in the carbon nanotubes.

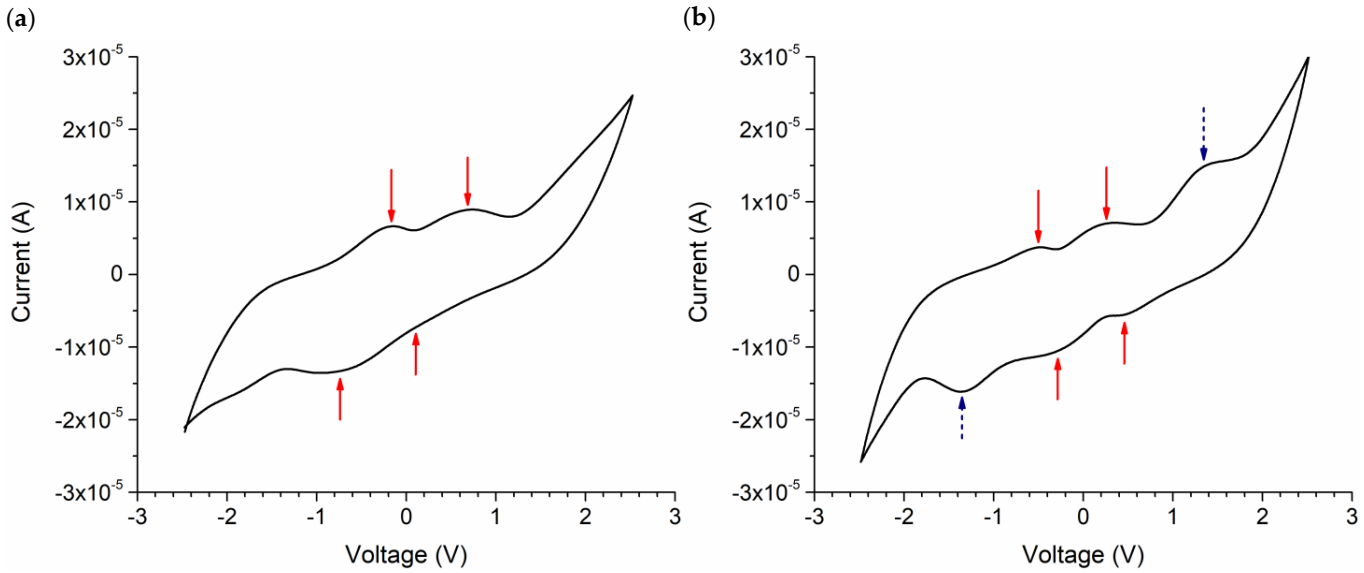

Figure 12. Cyclic voltammograms of membranes of (**a**) MWOHs and (**b**) RLi. The assembly of Figure 11 was used for the experiments. The red continuous arrows indicate processes of aluminum oxidation and dissolution, while the dashed arrows indicate processes of Li-Al alloying/de-alloying.

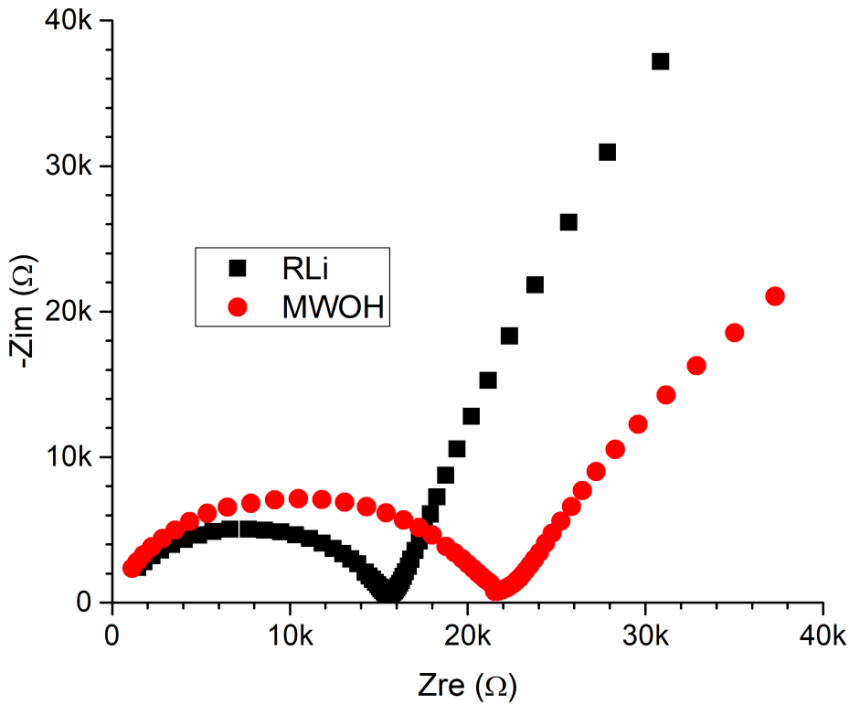

Figure 13. Impedance spectroscopy spectra of the assembly of Figure 11 using membranes of MWOHs and RLi.

The pairs of peaks close to 0 V may be related to the oxidation and dissolution of aluminum. It has been reported that the Al deposition and dissolution occur at about 0.35 V when using a three-Al electrode electrochemical cell and an Al ion-conducting electrolyte [102]. On the other hand, double oxidation and reduction peaks with a potential difference of about 0.4 V have been observed using an Al_2O_3 working electrode in aqueous solution [132]. The voltammetry peaks shifted depending on the pH of the solution. The peaks most probably appeared due to the oxidation and dissolution of Al in alkaline and acidic solutions. The findings of the past two reports could be supported by the theory of Al electrochemical etching. Depending on the conditions of the electrolyte (conductivity, pH, viscosity, etc.), it is possible to change the potential of the electrochemical cell, producing either oxidation or dissolution of Al and aluminum oxides, or a combination of both processes [133].

Additionally, the RLi sample presents an oxidation–reduction couple at higher potentials (indicated with dashed arrows in Figure 12b). These peaks appear at ±1.34 V. These peaks may be related to the alloying/de-alloying process of Li with Al. Using nanostructured Al as an electrode in a Li ion battery, it has been possible to have Li storage through the formation of Li-Al alloys. The difference in potential between Al and Li-Al alloys has been reported as 0.5 V in water-free Li ion-conducting electrolytes [134]. In the present case, the difference in potential is larger; however, it is well known that the nature of the electrolyte could have an effect on the potential of the battery. For example, when using a water-containing polymer electrolyte of polymethylmetacrylate in a Li ion battery, it was possible to change the voltage of the battery from 3 to 3.86 V when the electrolyte was UV-cured [135]. The fact that Al-Li alloying occurs is an indication that the lithiated carbon nanotubes could work as a source of Li ions and that these ions could be transported through the chitosan–starch matrix.

4. Conclusions

This comprehensive analysis involving XPS, FTIR and Raman spectroscopies and HRTEM effectively validated the successful oxidation and lithium modification of multi-walled carbon nanotubes. Notably, the presence of hydroxyl and carbonyl groups within oxidized multi-walled carbon nanotubes facilitates the binding of lithium ions originating from LiOH. Particularly, the carbon nanotubes lithiated with the reflux methodology exhibit good Li incorporation while oxidation is minimized, maintaining the graphitic character. Such nanotubes are optimal for Li ion exchange and electron transfer.

Furthermore, the discernible enhancement in mechanical strength, as evidenced by the storage modulus measured through dynamic mechanical analysis (DMA), is particularly pronounced in the polymeric membranes with MWOHs compared to the ones with MWNTs. Thus, some oxidation of the carbon nanotubes is positive. This enhancement is reflected in the dispersion of carbon nanostructures within the biopolymer matrix, as observed in SEM micrographs.

Electrochemical characterization in symmetrical cells with Al current collectors indicates an enhancement in ionic transport through the membranes when the carbon nanotubes are lithiated. On the other hand, Al-Li alloying was inferred, indicating that the lithiated carbon nanotubes could work as a source of Li ions and that these ions could be transported through the chitosan–starch matrix.

Author Contributions: Y.E.-M.: writing—original draft, conceptualization, formal analysis, funding acquisition. E.Q.-G.: writing—review and editing, supervision, formal analysis, validation, resources. E.C.-Y.: investigation, data curation. S.D.-T.: supervision, resources. D.A.-L.: data curation. E.C.-M.: resources, data curation. R.P.-G.: investigation. J.B.-T.: investigation, resources. V.C.-M.: project administration, supervision, conceptualization, funding acquisition. All authors have read and agreed to the published version of the manuscript.

Funding: Y.E.-M., thanks the economic support of Consejo de Ciencia y Tecnología del Estado de Puebla (CONCyTEP) and Tecnológico Nacional de México through the 2021 Call for Projects of Technological Development and Innovation (Project: Caracterización y Ensamble de Baterías Li-S con Nanotubos de Carbono de Multipared Funcionalizados). On the other hand, E.Q.-G., thanks the economic support of Vicerrectoría de Investigación y Estudios de Posgrado of BUAP (VIEP-BUAP) through the project 00185-VIEP2023 and the National Council of Science and Technology (CONACyT) through the project of Frontiers of Science 21077 and the project PRONACES 316537.

Data Availability Statement: The data sets used to support the findings of this study are included within the article and are available from the corresponding author upon request.

Acknowledgments: The authors are indebted to Alejandra Núñez Pineda of Universidad Nacional Autónoma de México and Gustavo López Téllez of Universidad Autónoma del Estado de México for their technical support with synthesis activities, and FTIR, Raman and XPS characterization.

Conflicts of Interest: The authors declare that there are no conflicts of interest regarding the publication of this paper.

References

1. Neumann, J.; Petranikova, M.; Meeus, M.; Gamarra, J.D.; Younesi, R.; Winter, M.; Nowak, S. Recycling of Lithium-Ion Batteries—Current State of the Art, Circular Economy, and Next Generation Recycling. *Adv. Energy Mater.* **2022**, *12*, 2102917. [CrossRef]
2. Thauer, E.; Ottmann, A.; Schneider, P.; Möller, L.; Deeg, L.; Zeus, R.; Wilhelmi, F.; Schlestein, L.; Neef, C.; Ghunaim, R.; et al. Filled Carbon Nanotubes as Anode Materials for Lithium-Ion Batteries. *Molecules* **2020**, *25*, 1064. [CrossRef] [PubMed]
3. Seman, R.N.A.R.; Azam, M.A.; Mohamad, A.A. Systematic Gap Analysis of Carbon Nanotube-Based Lithium-Ion Batteries and Electrochemical Capacitors. *Renew. Sustain. Energy Rev.* **2017**, *75*, 644–659. [CrossRef]
4. Arya, A.; Sharma, A.L. Polymer Electrolytes for Lithium Ion Batteries: A Critical Study. *Ionics* **2017**, *23*, 497–540. [CrossRef]
5. Long, L.; Wang, S.; Xiao, M.; Meng, Y. Polymer Electrolytes for Lithium Polymer Batteries. *J. Mater. Chem. A* **2016**, *4*, 10038–10069. [CrossRef]
6. Croce, F.; Curini, R.; Martinelli, A.; Persi, L.; Ronci, F.; Scrosati, B.; Caminiti, R. Physical and Chemical Properties of Nanocomposite Polymer Electrolytes. *J. Phys. Chem. B* **1999**, *103*, 10632–10638. [CrossRef]
7. Chávez, E.L.; Oviedo-Roa, R.; Contreras-Pérez, G.; Martínez-Magadán, J.M.; Castillo-Alvarado, F.L. Theoretical Studies of Ionic Conductivity of Crosslinked Chitosan Membranes. *Int. J. Hydrogen Energy* **2010**, *35*, 12141–12146. [CrossRef]
8. Ma, J.; Sahai, Y.; Buchheit, R.G. Evaluation of Multivalent Phosphate Cross-Linked Chitosan Biopolymer Membrane for Direct Borohydride Fuel Cells. *J. Power Sources* **2012**, *202*, 18–27. [CrossRef]
9. Putri, Z.; Arcana, I.M. Biodegradation Test of SPS-LS Blends as Polymer Electrolyte Membrane Fuel Cells. In *AIP Conference Proceedings, Proceedings of the 4th International Conference on Mathematics and Natural Sciences (ICMNS 2012): Science for Health, Food and Sustainable Energy, Bandung, Indonesia, 8–9 November 2012*; American Institute of Physics Inc.: New York, NY, USA, 2014; Volume 1589, pp. 266–271.
10. Ji, D.; Park, J.M.; Oh, M.S.; Nguyen, T.L.; Shin, H.; Kim, J.S.; Kim, D.; Park, H.S.; Kim, J. Superstrong, Superstiff, and Conductive Alginate Hydrogels. *Nat. Commun.* **2022**, *13*, 3019. [CrossRef]
11. Liu, P.; Sherman, E.; Jacobsen, A. Design and Fabrication of Multifunctional Structural Batteries. *J. Power Sources* **2009**, *189*, 646–650. [CrossRef]
12. Song, J.Y.; Wang, Y.Y.; Wan, C.C. Review of Gel-Type Polymer Electrolytes for Lithium-Ion Batteries. *J. Power Sources* **1999**, *77*, 183–197. [CrossRef]
13. Shukur, M.F.; Ithnin, R.; Kadir, M.F.Z. Electrical Properties of Proton Conducting Solid Biopolymer Electrolytes Based on Starch–Chitosan Blend. *Ionics* **2013**, *20*, 977–999. [CrossRef]
14. Isa, M.I.N.; Samsudin, A.S. Potential Study of Biopolymer-Based Carboxymethylcellulose Electrolytes System for Solid-State Battery Application. *Int. J. Polym. Mater. Polym. Biomater.* **2016**, *65*, 561–567. [CrossRef]
15. Sudhakar, Y.N.; Selvakumar, M. Lithium Perchlorate Doped Plasticized Chitosan and Starch Blend as Biodegradable Polymer Electrolyte for Supercapacitors. *Electrochim. Acta* **2012**, *78*, 398–405. [CrossRef]
16. Raffaelle, R.P.; Gennett, T.; Maranchi, J.; Kumta, P.; Hepp, A.F.; Heben, M.J.; Dillon, A.C.; Jones, K.C. Carbon Nanotube Anodes for Lithium Ion Batteries. *Mater. Res. Soc. Symp. Proc.* **2002**, *706*, 343–349. [CrossRef]
17. Touhara, H.; Komiyama, S. Potential Use of Carbon Nanotubes as Anode Materials for Lithium Batteries. *Electrochemistry* **2003**, *71*, 877–882. [CrossRef]
18. Prompun, P.; Ratchahat, S.; Kaveevivitchai, W.; Kooamornpattana, W. Carbon Nanotube (CNTs) Production from Waste Cooking Oil As Anode Material for Li-Ion Batteries. *J. Phys. Conf. Ser.* **2022**, *2175*, 012041. [CrossRef]
19. Liang, M.; Liu, J.; O'Shea, A.; Nicolosi, V. Constructing Hierarchical Porous Structure in Microsized Silicon/Carbon Nanotubes Composite Anode with LiF-Rich Solid-Electrolyte Interfaces for Highly Stable Lithium-Ion Batteries. *J. Phys. Mater.* **2023**, *6*, 014003. [CrossRef]

20. Christwardana, M.; Septevani, A.A.; Yoshi, L.A. Sustainable Electricity Generation from Photo-Bioelectrochemical Cell Based on Carbon Nanotubes and Chlorophyll Anode. *Sol. Energy* **2021**, *227*, 217–223. [CrossRef]
21. Liu, Z. Fabrication of Polymer Based on Carbon Nanotube Electrospun Nanofibers as Anode for High-Performance Li-Ion Battery. *Int. J. Electrochem. Sci.* **2022**, *17*, 221125. [CrossRef]
22. Li, X.; Xue, C.; Liu, Y.; Zhao, J.; Zhang, J.; Zhang, J. Amorphous Structure and Sulfur Doping Synergistically Inducing Defect-Rich Short Carbon Nanotubes as a Superior Anode Material in Lithium-Ion Batteries. *Electrochim. Acta* **2023**, *440*, 141697. [CrossRef]
23. Varshney, P.K.; Gupta, S. Natural Polymer-Based Electrolytes for Electrochemical Devices: A Review. *Ionics* **2011**, *17*, 479–483. [CrossRef]
24. Muthukrishnan, M.; Shanthi, C.; Selvasekarapandian, S.; Premkumar, R. Biodegradable Flexible Proton Conducting Solid Biopolymer Membranes Based on Pectin and Ammonium Salt for Electrochemical Applications. *Int. J. Hydrogen Energy* **2023**, *48*, 5387–5401. [CrossRef]
25. Awang, F.F.; Hassan, M.F.; Kamarudin, K.H. Investigation of Structural and Electrical Properties of a Biopolymer Materials with Its Potential Application in Solid-State Batteries. *Polym. Bull.* **2023**, *80*, 1463–1476. [CrossRef]
26. Vásconez, M.B.; Flores, S.K.; Campos, C.A.; Alvarado, J.; Gerschenson, L.N. Antimicrobial Activity and Physical Properties of Chitosan–Tapioca Starch Based Edible Films and Coatings. *Food Res. Int.* **2009**, *42*, 762–769. [CrossRef]
27. Castrejón-Parga, K.Y.; Camacho-Montes, H.; Rodríguez-González, C.A.; Velasco-Santos, C.; Martínez-Hernández, A.L.; Bueno-Jaquez, D.; Rivera-Armenta, J.L.; Ambrosio, C.R.; Conzalez, C.C.; Mendoza-Duarte, M.E. Chitosan–Starch Film Reinforced with Magnetite-Decorated Carbon Nanotubes. *J. Alloys Compd.* **2014**, *615*, S505–S510. [CrossRef]
28. Liu, H.; Adhikari, R.; Guo, Q.; Adhikari, B. Preparation and Characterization of Glycerol Plasticized (High-Amylose) Starch–Chitosan Films. *J. Food Eng.* **2013**, *116*, 588–597. [CrossRef]
29. Yan, L.; Chang, P.R.; Zheng, P. Preparation and Characterization of Starch-Grafted Multiwall Carbon Nanotube Composites. *Carbohydr. Polym.* **2011**, *84*, 1378–1383. [CrossRef]
30. Deepthi, M.V.; Ananthapadmanabha, G.S.; Sampathkumaran, P.; Seetharamu, S.; Pattenshetti, V.V.; Ganga, S.; Asai Thambi, V.; Sailaja, R.R.N. Preparation of Bio-Nanocomposites of Chitosan/Thermoplastic Starch Reinforced with Multiwalled Carbon Nanotubes. In Proceedings of the 2012 IEEE 10th International Conference on the Properties and Applications of Dielectric Materials (ICPADM), Bangalore, India, 24–28 July 2012; IEEE: New York, NY, USA, 2012; pp. 1–4.
31. Xie, F.; Pollet, E.; Halley, P.J.; Averous, L. Starch-Based Nano-Biocomposites. *Prog. Polym. Sci.* **2013**, *38*, 1590–1628. [CrossRef]
32. Wan, Y.; Creber, K.A.M.; Peppley, B.; Bui, V.T. Ionic Conductivity of Chitosan Membranes. *Polymer* **2003**, *44*, 1057–1065. [CrossRef]
33. Wang, Z.; Liu, J.; Zhang, J.; Hao, S.; Duan, X.; Song, H.; Zhang, J. Novel Chemically Cross-Linked Chitosan-Cellulose Based Ionogel with Self-Healability, High Ionic Conductivity, and High Thermo-Mechanical Stability. *Cellulose* **2020**, *27*, 5121–5133. [CrossRef]
34. Yadav, M.; Verma, A.; Nautiyal, G.; Srivastava, N. Magnesium Perchlorate Mixed and Glutaraldehyde Crosslinked Potato Starch: An Economical and Flexible Electrolyte Membrane. *Macromol. Sympos.* **2019**, *388*, 1900033. [CrossRef]
35. Koduru, H.K.; Marinov, Y.G.; Kaleemulla, S.; Rafailov, P.M.; Hadjichristov, G.B.; Scaramuzza, N. Fabrication and Characterization of Magnesium—Ion-Conducting Flexible Polymer Electrolyte Membranes Based on a Nanocomposite of Poly(Ethylene Oxide) and Potato Starch Nanocrystals. *J. Solid State Electrochem.* **2021**, *25*, 2409–2428. [CrossRef]
36. Zhou, L.; Liu, S.; Li, W.; Song, H.; Du, L.; Cui, Z. Highly Conductive Poly(ε-Caprolactone) and Chitosan Based Polymer Electrolyte for Lithium Metal Battery. *J. Power Sources* **2023**, *553*, 232271. [CrossRef]
37. Yusof, Y.M.; Shukur, M.F.; Illias, H.A.; Kadir, M.F.Z. Conductivity and Electrical Properties of Corn Starch-Chitosan Blend Biopolymer Electrolyte Incorporated with Ammonium Iodide. *Phys. Scr.* **2014**, *89*, 035701. [CrossRef]
38. Majumdar, S.; Sen, P.; Ray, R. Ionic Interactions and Transport Properties in Chitosan-Starch Based Blend Solid Biopolymer Electrolytes. *Mater. Today Proc.* **2019**, *18*, 4913–4920. [CrossRef]
39. Majumdar, S.; Sen, P.; Ray, R. High-Performance Graphene Oxide-Grafted Chitosan-Starch Solid Biopolymer Electrolytes for Flexible Hybrid Supercapacitors. *J. Solid State Electrochem.* **2022**, *26*, 527–547. [CrossRef]
40. Ding, L.; Leones, R.; Omar, A.; Guo, J.; Lu, Q.; Oswald, S.; Nielsch, K.; Giebeler, L.; Mikhailova, D. Highly Efficient Multicomponent Gel Biopolymer Binder Enables Ultrafast Cycling and Applicability in Diverse Battery Formats. *ACS Appl. Mater. Interfaces* **2020**, *12*, 53827–53840. [CrossRef]
41. Zeng, X.; Sun, X.; Cheng, G.; Yan, X.; Xu, X. Production of Multi-Wall Carbon Nanotubes on a Large Scale. *Phys. B Condens. Matter* **2002**, *323*, 330–332. [CrossRef]
42. Spitalsky, Z.; Tasis, D.; Papagelis, K.; Galiotis, C. Carbon Nanotube–Polymer Composites: Chemistry, Processing, Mechanical and Electrical Properties. *Prog. Polym. Sci.* **2010**, *35*, 357–401. [CrossRef]
43. Osswald, S.; Havel, M.; Gogotsi, Y. Monitoring Oxidation of Multiwalled Carbon Nanotubes by Raman Spectroscopy. *J. Raman Spectrosc.* **2007**, *38*, 728–736. [CrossRef]
44. Hong, C.-E.; Lee, J.-H.; Kalappa, P.; Advani, S.G. Effects of Oxidative Conditions on Properties of Multi-Walled Carbon Nanotubes in Polymer Nanocomposites. *Compos. Sci. Technol.* **2007**, *67*, 1027–1034. [CrossRef]
45. Yu, H.; Jin, Y.; Peng, F.; Wang, H.; Yang, J. Kinetically Controlled Side-Wall Functionalization of Carbon Nanotubes by Nitric Acid Oxidation. *J. Phys. Chem. C* **2008**, *112*, 6758–6763. [CrossRef]
46. Zhang, J.; Zou, H.; Qing, Q.; Yang, Y.; Li, Q.; Liu, Z.; Guo, X.; Du, Z. Effect of Chemical Oxidation on the Structure of Single-Walled Carbon Nanotubes. *J. Phys. Chem. B* **2003**, *107*, 3712–3718. [CrossRef]

47. Hung, T.-C.; Chen, C.-F.; Chen, M.; Chen, C.-C. Quantitative Limitation of Active Site and Characteristics of Chemical Oxidized Well-Aligned Carbon Nanotubes. *Thin Solid Film.* **2008**, *516*, 5236–5240. [CrossRef]
48. Jaunsen, J.R. *The Behavior and Capabilities of Lithium Hydroxide Carbon Dioxide Scrubbers in a Deep Sea Environment*; Naval Academy: Annapolis, MD, USA, 1989.
49. Ai, J.; Rezaei-Tavirani, M.; Biazar, E.; Heidari, K.S.; Jahandideh, R. Mechanical Properties of Chitosan-Starch Composite Filled Hydroxyapatite Micro-and Nanopowders. *J. Nanomater.* **2011**, *2011*, 16. [CrossRef]
50. Tuhin, M.O.; Rahman, N.; Haque, M.E.; Khan, R.A.; Dafader, N.C.; Islam, R.; Nurnabi, M.; Tonny, W. Modification of Mechanical and Thermal Property of Chitosan–Starch Blend Films. *Radiat. Phys. Chem.* **2012**, *81*, 1659–1668. [CrossRef]
51. Espíndola-González, A.; Martínez-Hernández, A.L.; Fernández-Escobar, F.; Castaño, V.M.; Brostow, W.; Datashvili, T.; Velasco-Santos, C. Natural-Synthetic Hybrid Polymers Developed via Electrospinning: The Effect of PET in Chitosan/Starch System. *Int. J. Mol. Sci.* **2011**, *12*, 1908–1920. [CrossRef]
52. Liu, H.; Yu, L.; Dean, K.; Simon, G.; Petinakis, E.; Chen, L. Starch Gelatinization under Pressure Studied by High Pressure DSC. *Carbohydr. Polym.* **2009**, *75*, 395–400. [CrossRef]
53. Belin, T.; Epron, F. Characterization Methods of Carbon Nanotubes: A Review. *Mater. Sci. Eng. B* **2005**, *119*, 105–118. [CrossRef]
54. Kuhlmann, U.; Jantoljak, H.; Pfänder, N.; Bernier, P.; Journet, C.; Thomsen, C. Infrared Active Phonons in Single-Walled Carbon Nanotubes. *Chem. Phys. Lett.* **1998**, *294*, 237–240. [CrossRef]
55. Aqel, A.; El-Nour, K.M.; Ammar, R.A.; Al-Warthan, A. Carbon Nanotubes, Science and Technology Part (I) Structure, Synthesis and Characterisation. *Arab. J. Chem.* **2012**, *5*, 1–23. [CrossRef]
56. McCreery, R.L. Advanced Carbon Electrode Materials for Molecular Electrochemistry. *Chem. Rev.* **2008**, *108*, 2646–2687. [CrossRef] [PubMed]
57. Estévez-Martínez, Y.; Velasco-Santos, C.; Martínez-Hernández, A.-L.; Delgado, G.; Cuevas-Yáñez, E.; Alaníz-Lumbreras, D.; Duron-Torres, S.; Castaño, V.M. Grafting of Multiwalled Carbon Nanotubes with Chicken Feather Keratin. *J. Nanomater.* **2013**, *2013*, 38. [CrossRef]
58. Stobinski, L.; Lesiak, B.; Kövér, L.; Tóth, J.; Biniak, S.; Trykowski, G.; Judek, J. Multiwall Carbon Nanotubes Purification and Oxidation by Nitric Acid Studied by the FTIR and Electron Spectroscopy Methods. *J. Alloys Compd.* **2010**, *501*, 77–84. [CrossRef]
59. Lehman, J.H.; Terrones, M.; Mansfield, E.; Hurst, K.E.; Meunier, V. Evaluating the Characteristics of Multiwall Carbon Nanotubes. *Carbon* **2011**, *49*, 2581–2602. [CrossRef]
60. Verma, P.; Maire, P.; Novák, P. A Review of the Features and Analyses of the Solid Electrolyte Interphase in Li-Ion Batteries. *Electrochim. Acta* **2010**, *55*, 6332–6341. [CrossRef]
61. Naudin, C.; Bruneel, J.L.; Chami, M.; Desbat, B.; Grondin, J.; Lassègues, J.C.; Servant, L. Characterization of the Lithium Surface by Infrared and Raman Spectroscopies. *J. Power Sources* **2003**, *124*, 518–525. [CrossRef]
62. Karakassides, M.A.; Gournis, D.; Petridis, D. An Infrared Reflectance Study of Si-O Vibrations in Thermally Treated Alkalisaturated Montmorillonites. *Clay Miner.* **1999**, *34*, 429–438. [CrossRef]
63. Morigaki, K.-I.; Ohta, A. Analysis of the Surface of Lithium in Organic Electrolyte by Atomic Force Microscopy, Fourier Transform Infrared Spectroscopy and Scanning Auger Electron Microscopy. *J. Power Sources* **1998**, *76*, 159–166. [CrossRef]
64. Aurbach, D.; Markovsky, B.; Weissman, I.; Levi, E.; Ein-Eli, Y. On the Correlation between Surface Chemistry and Performance of Graphite Negative Electrodes for Li Ion Batteries. *Electrochim. Acta* **1999**, *45*, 67–86. [CrossRef]
65. Radziemski, L.J.; Engleman, R., Jr.; Brault, J.W. Fourier-Transform-Spectroscopy Measurements in the Spectra of Neutral Lithium, I6 and I7 (Li I). *Phys. Rev. A* **1995**, *52*, 4462–4470. [CrossRef] [PubMed]
66. Kim, J.; Kim, M.; Noh, S.; Lee, G.; Shin, D. Enhanced Electrochemical Performance of Surface Modified LiCoO2 for All-Solid-State Lithium Batteries. *Ceram. Int.* **2016**, *42*, 2140–2146. [CrossRef]
67. Ferraro, J.R. *Introductory Raman Spectroscopy*; Academic Press: New York, NY, USA, 2003; ISBN 0-08-05091-26.
68. Jantoljak, H.; Salvetat, J.-P.; Forró, L.; Thomsen, C. Low-Energy Raman-Active Phonons of Multiwalled Carbon Nanotubes. *Appl. Phys. A Mater. Sci. Process.* **1998**, *67*, 113–116. [CrossRef]
69. Efremov, E.V.; Ariese, F.; Gooijer, C. Achievements in Resonance Raman Spectroscopy. Review of a Technique with a Distinct Analytical Chemistry Potential. *Anal. Chim. Acta* **2008**, *606*, 119–134. [CrossRef] [PubMed]
70. Wang, X.; Wang, C.; Cheng, L.; Lee, S.-T.; Liu, Z. Noble Metal Coated Single-Walled Carbon Nanotubes for Applications in Surface Enhanced Raman Scattering Imaging and Photothermal Therapy. *J. Am. Chem. Soc.* **2012**, *134*, 7414–7422. [CrossRef]
71. Sato-Berrú, R.Y.; Basiuk, E.V.; Saniger, J.M. Application of Principal Component Analysis to Discriminate the Raman Spectra of Functionalized Multiwalled Carbon Nanotubes. *J. Raman Spectrosc.* **2006**, *37*, 1302–1306. [CrossRef]
72. Thomsen, C.; Reich, S. *Raman Scattering in Carbon Nanotubes*; Topics in Applied Physics: Berlin, Germany, 2006; Volume 108.
73. Kataura, H.; Achiba, Y.; Zhao, X.; Ando, Y. Resonance Raman Scattering of Multi-Walled Carbon Nanotubes. *MRS Online Proc. Libr.* **2000**, *593*, 113–118. [CrossRef]
74. Athalin, H.; Lefrant, S. A Correlated Method for Quantifying Mixed and Dispersed Carbon Nanotubes: Analysis of the Raman Band Intensities and Evidence of Wavenumber Shift. *J. Raman Spectrosc.* **2005**, *36*, 400–408. [CrossRef]
75. Dresselhaus, M.S.; Dresselhaus, G.; Hofmann, M. The Big Picture of Raman Scattering in Carbon Nanotubes. *Vib. Spectrosc.* **2007**, *45*, 71–81. [CrossRef]
76. Gupta, S.; Patel, R.J. Changes in the Vibrational Modes of Carbon Nanotubes Induced by Electron-Beam Irradiation: Resonance Raman Spectroscopy. *J. Raman Spectrosc.* **2007**, *38*, 188–199. [CrossRef]

77. Jorio, A.; Saito, R.; Dresselhaus, G.; Dresselhaus, M.S. Determination of Nanotubes Properties by Raman Spectroscopy. *Philos. Trans. R. Soc. A Math. Phys. Eng. Sci.* **2004**, *362*, 2311–2336. [CrossRef] [PubMed]
78. Delhaes, P.; Couzi, M.; Trinquecoste, M.; Dentzer, J.; Hamidou, H.; Vix-Guterl, C. A Comparison between Raman Spectroscopy and Surface Characterizations of Multiwall Carbon Nanotubes. *Carbon* **2006**, *44*, 3005–3013. [CrossRef]
79. Heise, H.M.; Kuckuk, R.; Ojha, A.K.; Srivastava, A.; Srivastava, V.; Asthana, B.P. Characterisation of Carbonaceous Materials Using Raman Spectroscopy: A Comparison of Carbon Nanotube Filters, Single- and Multi-Walled Nanotubes, Graphitised Porous Carbon and Graphite. *J. Raman Spectrosc.* **2009**, *40*, 344–353. [CrossRef]
80. Zdrojek, M.; Gebicki, W.; Jastrzebski, C.; Melin, T.; Huczko, A. Studies of Multiwall Carbon Nanotubes Using Raman Spectroscopy and Atomic Force Microscopy. *Solid State Phenom.* **2004**, *99–100*, 265–268. [CrossRef]
81. Dresselhaus, M.S.; Dresselhaus, G.; Saito, R.; Jorio, A. Raman Spectroscopy of Carbon Nanotubes. *Phys. Rep.* **2005**, *409*, 47–99. [CrossRef]
82. Dresselhaus, M.S.; Jorio, A.; Souza Filho, A.G.; Saito, R. Defect Characterization in Graphene and Carbon Nanotubes Using Raman Spectroscopy. *Philos. Trans. R. Soc. A* **2010**, *368*, 5355–5377. [CrossRef]
83. Nishide, D.; Miyata, Y.; Yanagi, K.; Tanaka, T.; Kataura, H. PERIPUTOS: Purity Evaluated by Raman Intensity of Pristine and Ultracentrifuged Topping of Single-Wall Carbon Nanotubes. *Phys. Status Solidi B Basic Res.* **2009**, *246*, 2728–2731. [CrossRef]
84. Irurzun, V.M.; Ruiz, M.P.; Resasco, D.E. Raman Intensity Measurements of Single-Walled Carbon Nanotube Suspensions as a Quantitative Technique to Assess Purity. *Carbon* **2010**, *48*, 2873–2881. [CrossRef]
85. Kataura, H.; Miyata, Y.; Mizuno, K. Purity and Defect Characterization of Single-Wall Carbon Nanotubes Using Raman Spectroscopy. *J. Nanomater.* **2011**, *2011*, 786763.
86. Dillon, A.C.; Yudasaka, M.; Dresselhaus, M.S. Employing Raman Spectroscopy to Qualitatively Evaluate the Purity of Carbon Single-Wall Nanotube Materials. *J. Nanosci. Nanotechnol.* **2004**, *4*, 691–703. [CrossRef] [PubMed]
87. DiLeo, R.A.; Landi, B.J.; Raffaelle, R.P. Purity Assessment of Multiwalled Carbon Nanotubes by Raman Spectroscopy. *J. Appl. Phys.* **2007**, *101*, 064307. [CrossRef]
88. Hernandez-Ortiz, M.; Estevez-Martínez, Y.; Durón, S.; Escalante-García, I.; Vega-González, M.; Castaño, V. Morphology and Surface Structure of Nanocarbon Allotropes: A Comparative Study. *Fuller. Nanotub. Carbon Nanostruct.* **2016**, *24*, 345–352. [CrossRef]
89. Rocha, R.P.; Sousa, J.P.S.; Silva, A.M.T.; Pereira, M.F.R.; Figueiredo, J.L. Catalytic Activity and Stability of Multiwalled Carbon Nanotubes in Catalytic Wet Air Oxidation of Oxalic Acid: The Role of the Basic Nature Induced by the Surface Chemistry. *Appl. Catal. B Environ.* **2011**, *104*, 330–336. [CrossRef]
90. Liu, X.; Wang, R.; Song, L.; He, H.; Zhang, G.; Zi, X.; Qiu, W. The Oxidation of Carbon Monoxide over the Palladium Nanocube Catalysts: Effect of the Basic-Property of the Support. *Catal. Commun.* **2014**, *46*, 213–218. [CrossRef]
91. Ingrosso, C.; Bianco, G.V.; Lopalco, P.; Tamborra, M.; Curri, M.L.; Corcelli, A.; Bruno, G.; Agostiano, A.; Siciliano, P.; Striccoli, M. Surface Chemical Functionalization of Single Walled Carbon Nanotubes with a Bacteriorhodopsin Mutant. *Nanoscale* **2012**, *4*, 6434–6441. [CrossRef] [PubMed]
92. Zhao, J.; Buldum, A.; Han, J.; Lu, J.P. First-Principles Study of Li-Intercalated Carbon Nanotube Ropes. *Phys. Rev. Lett.* **2000**, *85*, 1706–1709. [CrossRef]
93. Maurin, G.; Bousquet, C.; Henn, F.; Bernier, P.; Almairac, R.; Simon, B. Electrochemical Lithium Intercalation into Multiwall Carbon Nanotubes: A Micro-Raman Study. *Solid State Ion.* **2000**, *136–137*, 1295–1299. [CrossRef]
94. Kim, Y.A.; Kojima, M.; Muramatsu, H.; Umemoto, S.; Watanabe, T.; Yoshida, K.; Sato, K.; Ikeda, T.; Hayashi, T.; Endo, M.; et al. In Situ Raman Study on Single- and Double-Walled Carbon Nanotubes as a Function of Lithium Insertion. *Small* **2006**, *2*, 667–676. [CrossRef]
95. Maurin, G.; Henn, F.; Simon, B.; Colomer, J.-F.; Nagy, J.B. Lithium Doping of Multiwalled Carbon Nanotubes Produced by Catalytic Decomposition. *Nano Lett.* **2001**, *1*, 75–79. [CrossRef]
96. Li, J.; Wu, C.; Guan, L. Lithium Insertion/Extraction Properties of Nanocarbon Materials. *J. Phys. Chem. C* **2009**, *113*, 18431–18435. [CrossRef]
97. Ye, J.T.; Li, Z.M.; Tang, Z.K.; Saito, R. Raman Spectra of Lithium Doped Single-Walled 0.4 Nm Carbon Nanotubes. *Phys. Rev. B* **2003**, *67*, 1134041–1134044. [CrossRef]
98. Yoong, A.K.; Kojima, M.; Muramatsu, H.; Shimamoto, D.; Hayashi, T.; Endo, M.; Terrones, M.; Dresselhaus, M.S. Raman Study on Electrochemical Lithium Insertion into Multiwalled Carbon Nanotubes. *J. Raman Spectrosc.* **2008**, *39*, 1183–1188.
99. Müller, M.; Meinke, R.; Maultzsch, J.; Gebhardt, B.; Hauke, F.; Hirsch, A.; Thomsen, C. Resonant Raman Scattering on Carbon Nanotubes Covalently Functionalized with Lithium Decyne. *Phys. Status Solidi B Basic Res.* **2010**, *247*, 2863–2866. [CrossRef]
100. Porto, A.B.; Silva, G.G.; Dos Santos, H.F.; De Oliveira, L.F.C. Oxidation of Single-Walled Carbon Nanotubes under Controlled Chemical Conditions. *J. Braz. Chem. Soc.* **2018**, *29*, 2387–2396. [CrossRef]
101. Venkateswer Rao, M.; Dhand, V.; Sarada Prasad, J.; Naga Mahesh, K.; Himabindu, V.; Yerramilli, A.; Sreedhar, B. In Situ Lithium Intercalation of Carbon Nanorods Using Flame Synthesis. *Compos. Sci. Technol.* **2010**, *70*, 255–259. [CrossRef]
102. Santamaría-Juárez, G.; Gómez-Barojas, E.; Quiroga-González, E.; Sánchez-Mora, E.; Quintana-Ruiz, M.; Santamaría-Juárez, J.D. Safer Modified Hummers' Method for the Synthesis of Graphene Oxide with High Quality and High Yield. *Mater. Res. Express* **2020**, *6*, 125631. [CrossRef]

103. Maruyama, S.; Fukutsuka, T.; Miyazaki, K.; Abe, T. Solvated Lithium Ion Intercalation Behavior of Graphitized Carbon Nanospheres. *Electrochemistry* **2020**, *88*, 79–82. [CrossRef]
104. Schechter, A.; Aurbach, D.; Cohen, H. X-Ray Photoelectron Spectroscopy Study of Surface Films Formed on Li Electrodes Freshly Prepared in Alkyl Carbonate Solutions. *Langmuir* **1999**, *15*, 3334–3342. [CrossRef]
105. Kanamura, K.; Shiraishi, S.; Takezawa, H.; Takehara, Z. XPS Analysis of the Surface of a Carbon Electrode Intercalated by Lithium Ions. *Chem. Mater.* **1997**, *9*, 1797–1804. [CrossRef]
106. Aurbach, D.; Weissman, I.; Schechter, A.; Cohen, H. X-Ray Photoelectron Spectroscopy Studies of Lithium Surfaces Prepared in Several Important Electrolyte Solutions. A Comparison with Previous Studies by Fourier Transform Infrared Spectroscopy. *Langmuir* **1996**, *12*, 3991–4007. [CrossRef]
107. Ismail, I.; Noda, A.; Nishimoto, A.; Watanabe, M. XPS Study of Lithium Surface after Contact with Lithium-Salt Doped Polymer Electrolytes. *Electrochim. Acta* **2001**, *46*, 1595–1603. [CrossRef]
108. Wu, Y.; Okajima, T.; Ohsaka, T. Lithium Intercalation into Graphene Ribbons of Glassy Carbon. *Int. J. Electrochem. Sci.* **2017**, *12*, 1004–1013. [CrossRef]
109. Canobre, S.C.; Bocchi, N.; Rocha-Filho, R.C.; Biaggio, S.R. Carbon-Fiber Composites of Organometallic Intercalated Polyaniline and Polypyrrole Doped with Sodium Polystyrene Sulfonate as Electrodes for Lithium-Ion Batteries. *Mater. Chem. Phys.* **2013**, *139*, 47–54. [CrossRef]
110. Reddy, S.S.; Shukla, B.; Srihari, V.; Bhalerao, G.M.; Shekar, N.V.C. Realization of Diamond Nucleation within the Multi-Walled Carbon Nanotubes Matrix upon Electron Irradiation. *Carbon Lett.* **2022**, *32*, 1119–1130. [CrossRef]
111. Zhang, H.; Sun, C.H.; Li, F.; Li, H.X.; Cheng, H.M. Purification of Multiwalled Carbon Nanotubes by Annealing and Extraction Based on the Difference in van Der Waals Potential. *J. Phys. Chem. B* **2006**, *110*, 9477–9481. [CrossRef]
112. Okoro, A.M.; Machaka, R.; Lephuthing, S.S.; Awotunde, M.A.; Olubambi, P.A. Microstructural Evolution and Mechanical Properties of Multiwall Carbon Nanotubes Reinforced Titanium-Based Nanocomposites Developed by Spark Plasma Sintering. *Met. Mater. Int.* **2021**, *27*, 4869–4885. [CrossRef]
113. Estévez-Martíneza, Y.; Velasco-Santos, C.; Martínez-Hernández, A.-L.; Delgado, G.; Arenas-Alatorre, J.; Durón-Torres, S.; Alaniz-Lumbreras, D.; Castaño, V.M. Characterization of Nanostructures of Oxidized Multiwalled Carbon Nanotubes –G–Keratin Hybrids by Transmission Electron Microscopy. *J. Nanosci. Lett.* **2015**, *5*, 10.
114. Bhattacharya, S.; Riahi, A.R.; Alpas, A.T. A Transmission Electron Microscopy Study of Crack Formation and Propagation in Electrochemically Cycled Graphite Electrode in Lithium-Ion Cells. *J. Power Sources* **2011**, *196*, 8719–8727. [CrossRef]
115. Che, B.D.; Nguyen, B.Q.; Nguyen, L.-T.T.; Nguyen, H.T.; Nguyen, V.Q.; Van Le, T.; Nguyen, N.H. The Impact of Different Multi-Walled Carbon Nanotubes on the X-Band Microwave Absorption of Their Epoxy Nanocomposites. *Chem. Cent. J.* **2015**, *9*, 10. [CrossRef]
116. Shah, M. Growth of Uniform Nanoparticles of Platinum by an Economical Approach at Relatively Low Temperature. *Sci. Iran* **2012**, *19*, 964–966. [CrossRef]
117. Johnsen, R.E.; Norby, P. Capillary-Based Micro-Battery Cell for in Situ X-Ray Powder Diffraction Studies of Working Batteries: A Study of the Initial Intercalation and Deintercalation of Lithium into Graphite. *J. Appl. Crystallog.* **2013**, *46*, 1537–1543. [CrossRef]
118. Brown, M.E.; Gallagher, P.K. *Handbook of Thermal Analysis and Calorimetry: Recent Advances, Techniques and Applications*; Elsevier: New York, NY, USA, 2011; Volume 5, ISBN 0-08-05563-10.
119. Skoog, D.A.; Holler, F.J.; Nieman, T.A.; del Gómez, M.C.M. *Principios de Análisis Instrumental*; McGraw-Hill Madrid: Madrid, Spain, 2001; ISBN 8-44-81277-57.
120. Flores-Hernández, C.G.; Martínez-Hernández, A.L.; Velasco-Santos, C. Chitosan-Starch Ecocomposites: Sustainable Biopolymer Matrix Reinforced with Green Fibers. In *Handbook of Sustainable Polymers: Structure and Chemistry*; Pan Stanford Publishing Pte Ltd.: Singapore, 2016; pp. 509–557, ISBN 978-9-81461-356-9.
121. Lazaridou, A.; Biliaderis, C.G. Thermophysical Properties of Chitosan, Chitosan-Starch and Chitosan-Pullulan Films near the Glass Transition. *Carbohydr. Polym.* **2002**, *48*, 179–190. [CrossRef]
122. Nicotera, I.; Simari, C.; Agostini, M.; Enotiadis, A.; Brutti, S. A Novel Li^+-Nafion-Sulfonated Graphene Oxide Membrane as Single Lithium-Ion Conducting Polymer Electrolyte for Lithium Batteries. *J. Phys. Chem. C* **2019**, *123*, 27406–27416. [CrossRef]
123. Stephan, A.M.; Kumar, T.P.; Kulandainathan, M.A.; Lakshmi, N.A. Chitin-Incorporated Poly(Ethylene Oxide)-Based Nanocomposite Electrolytes for Lithium Batteries. *J. Phys. Chem. B* **2009**, *113*, 1963–1971. [CrossRef] [PubMed]
124. Brouillet-Fourmann, S.; Carrot, C.; Mignard, N. Gelatinization and Gelation of Corn Starch Followed by Dynamic Mechanical Spectroscopy Analysis. *Rheol. Acta* **2003**, *42*, 110–117. [CrossRef]
125. Mathew, S.; Brahmakumar, M.; Abraham, T.E. Microstructural Imaging and Characterization of the Mechanical, Chemical, Thermal, and Swelling Properties of Starch-Chitosan Blend Films. *Biopolymers* **2006**, *82*, 176–187. [CrossRef]
126. Liu, F.; Qin, B.; He, L.; Song, R. Novel Starch/Chitosan Blending Membrane: Antibacterial, Permeable and Mechanical Properties. *Carbohydr. Polym.* **2009**, *78*, 146–150. [CrossRef]
127. Bourtoom, T.; Chinnan, M.S. Preparation and Properties of Rice Starch-Chitosan Blend Biodegradable Film. *LWT Food Sci. Technol.* **2008**, *41*, 1633–1641. [CrossRef]
128. López, F.A.; Mercê, A.L.R.; Alguacil, F.J.; López-Delgado, A. A Kinetic Study on the Thermal Behaviour of Chitosan. *J. Therm. Anal. Calorim.* **2008**, *91*, 633–639. [CrossRef]
129. Souza, N.L.G.D.; Brandão, H.M.; De Oliveira, L.F.C. Spectroscopic and Thermogravimetric Study of Chitosan after Incubation in Bovine Rumen. *J. Mol. Struct.* **2011**, *1005*, 186–191. [CrossRef]

130. Sugimoto, M.; Morimoto, M.; Sashiwa, H.; Saimoto, H.; Shigemasa, Y. Preparation and Characterization of Water-Soluble Chitin and Chitosan Derivatives. *Carbohydr. Polym.* **1998**, *36*, 49–59. [CrossRef]
131. Zou, M.-M.; Ai, D.-J.; Liu, K.-Y. Template Synthesis of MnO2/CNT Nanocomposite and Its Application in Rechargeable Lithium Batteries. *Trans. Nonferrous Met. Soc. China* **2011**, *21*, 2010–2014. [CrossRef]
132. Kusuma, K.B.; Manju, M.; Ravikumar, C.R.; Nagaswarupa, H.P.; Amulya, M.A.S.; Anilkumar, M.R.; Avinash, B.; Gurushantha, K.; Ravikantha, N. Photocatalytic and Electrochemical Sensor for Direct Detection of Paracetamol Comprising γ-Aluminium Oxide Nanoparticles Synthesized via Sonochemical Route. *Sens. Int.* **2020**, *1*, 100039. [CrossRef]
133. Poinern, G.E.J.; Ali, N.; Fawcett, D. Progress in Nano-Engineered Anodic Aluminum Oxide Membrane Development. *Materials* **2011**, *4*, 487–526. [CrossRef] [PubMed]
134. Hudak, N.; Huber, D. Nanostructured Lithium-Aluminum Alloy Electrodes for Lithium-Ion Batteries. *ECS Trans.* **2011**, *33*, 1–13. [CrossRef]
135. Badi, N.; Theodore, A.M.; Alghamdi, S.A.; Al-Aoh, H.A.; Lakhouit, A.; Singh, P.K.; Norrrahim, M.N.F.; Nath, G. The Impact of Polymer Electrolyte Properties on Lithium-Ion Batteries. *Polymers* **2022**, *14*, 3101. [CrossRef]